12-2017

Nanoenergetic Gas Generators Based on Metal Hydroxides

Srbuhi Yolchinyan
The University of Texas Rio Grande Valley

NANOENERGETIC GAS GENERATORS BASED ON METAL HYDROXIDES

A Thesis

by

SRBUHI YOLCHINYAN

Submitted to the Graduate College of
The University of Texas Rio Grande Valley
In partial fulfillment of the requirements for the degree of

MASTER OF SCIENCE

December 2017

Major Subject: Physics

NANOENERGETIC GAS GENERATORS BASED ON METAL HYDROXIDES

A Thesis
by
SRBUHI YOLCHINYAN

COMMITTEE MEMBERS

Dr. Karen Martirosyan
Chair of Committee

Dr. Ahmed Touhami
Committee Member

Dr. Myoung-Hwan Kim
Committee Member

December 2017

ABSTRACT

Yolchinyan, Srbuhi, Nanoenergetic Gas Generators based on Metal Hydroxides

Master of Science (MS), December, 2017, 71 pp., 1 table, 24 figures, references, 70 titles.

The metal oxide based nano thermites have been studied extensively, yet another closely related systems based on metal hydroxides were surprisingly overlooked. For the first time, the thermodynamic calculations using HSC Chemistry-7 and Thermo software, were performed for a collection of 22 novel nano-thermite systems based on aluminum and metal hydroxides, and four representative systems based on bismuth, copper, cerium and nickel hydroxides were characterized using differential scanning calorimeter, scanning electron microscope, and pressure discharge dynamic evaluation. The strongest performance was recorded in Al-$Bi(OH)_3$ system with about 4.9 MPa peak pressure for 0.2 g charge mass. Bismuth oxide and hydroxide particles resembling flowers, bowties and brushwood-like structures were successfully prepared via microfluidic synthesis approach. The formulation containing flower-shaped particles was superior to brushwood-like oxidizer, and produced the highest pressure discharge value of 14.3 MPa/g (4.9 kPa m^3 g^{-1}), which is comparable well to best reported values in literature.

DEDICATION

I would like to dedicate this thesis to my grandfather, Martun Yolchinyan, who has taught me to believe in myself, and whose good example motivates me to reach new heights in my life and career. This work is also dedicated to my parents, Armen Yolchinyan and Satenik Hakobyan, and to my son, Davit Hobosyan, who inspire me to work hard for the things that I aspire to achieve.

ACKNOWLEDGMENTS

I would like to thank my advisor, Dr. Karen Martirosyan, for his encouragement and guidance throughout my education and research. I gained invaluable knowledge and professional experience while working with him. I would also like to thank the members of my committee Dr. Ahmed Touhami and Dr. Myoung-Hwan Kim for taking the time and effort to take part in my thesis defense. I want to acknowledge the support of Mkhitar Hobosyan, who helped me to design and perform the experiments with nanoenergetic materials.

TABLE OF CONTENTS

LIST OF TABLES

Page

LIST OF FIGURES

Page

CHAPTER I

INTRODUCTION

1.1 Thermites

Thermites have been known since 19th century (Arnáiz et al, 1998). The thermite reaction was discovered in 1893 and patented in 1895 by the German Chemist Hans Goldschmidt. Thermites can have diverse class of compositions, as well as particle size ranging from nano-sized to up to 100 μm. The most famous thermite reaction is between aluminum and iron oxide, where the aluminum reduces iron oxide Fe_2O_3 producing Al_2O_3 and melted iron, and releases large amount of heat, according to the following reaction:

$$2Al + Fe_2O_3 = Al_2O_3 + 2Fe + \Delta H,\ \Delta H = -3.97\ kJ/g \qquad (1\text{-}1)$$

which was widely used in thermite welding of railroad tracks, and first track welding performed in 1899 in Essen, Germany. The thermites have been traditionally used not only for welding, but for metal cutting, disabling artillery pieces, etc. In some applications include the elementary metal production, such as aluminum-chromium oxide mixture, or copper oxide, which is used to produce joints during cad welding processes.

1.2. Nanostructured thermites

Recently, the thermites at nano-scale have focused much attention in scientific community. The so-called Nano-thermites are energetic formulations of metallic fuel and oxidizer particles, where at least one constituent should be in nano-size domain (Dlott 2006,

Martirosyan (2011), Sullivan (2010). The oxidizers include traditional metal oxides such as Co_3O_4, Fe_2O_3, CuO, MoO_3, etc (Patel et al (2015), Cheng et al (2010), Stamatis et al (2008), Umbrajkar et al (2006), as well as highly powerful Nanoenergetic Gas Generator (NGG) (Martirosyan et al, 2009) components such as iodine pentoxide I_2O_5 (Martirosyan et al (2009), Clark et al (2009), Hobosyan et al (2012), Hobosyan et al (2017), and bismuth trioxide Bi_2O_3 (Martirosyan 2009, Patel et al (2015), Puszynski et al (2007), Wang et al (2011). Aluminum is one of the most popular metals utilized as a fuel, although Mg is also used occasionally (Wang et al 2014, Zhou et al, 2014). The reason behind the popularity of aluminum as a fuel that Al is one of the cheapest metals to produce, is highly reactive, and has relatively low melting point (660 ^oC), which implies that it can easily melt and react with oxidizers in liquid form, tremendously accelerating the reaction rate in comparison to solid-solid reactions. Although aluminum is highly reactive, the aluminum oxide layer which naturally forms on aluminum particles, protects the aluminum core and makes it safer to handle even for 50-100 nm particle size.

The thermites at nano-scale have very high chemical reaction rate in comparison to thermites at micro-scale. When reducing the particle size to nano-meter domain, the reaction propagation velocity can increase by up to 2-3 orders of magnitude for some systems (Kim et al, 2014, Perry et al, 2004, Umbrajkar et al, 2006, Dreizin (2009), making them comparable or even better than the traditional energetic materials such as explosives and primers, including 2,4,6-trinitrotoluene (TNT), pentaerythritol tetranitrate (PETN), and 1,3,5-trinitroperhydro-1,3,5-triazine (RDX). The reason behind is that the nano-thermite systems have higher volumetric energy density compared to traditional energetic materials (Martirosyan, 2012).

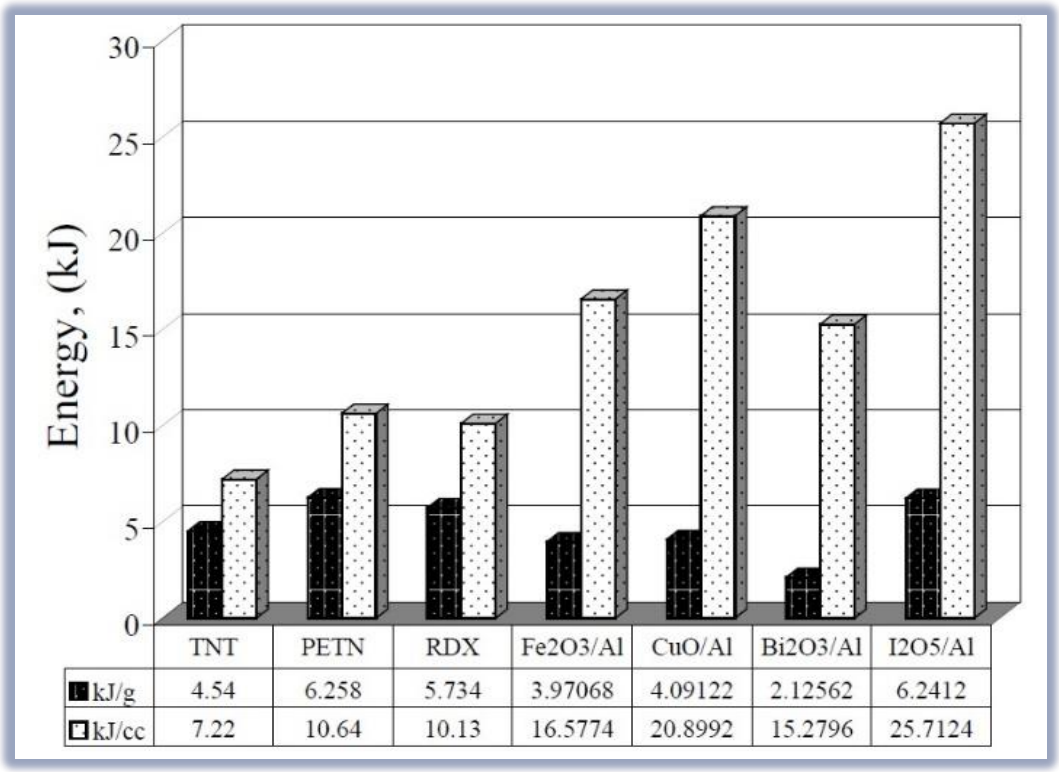

Figure 1. Comparison of energy release between the conventional energetic materials and thermite compositions (Copyright -Martirosyan, K (2012), used by permission).

Figure 1 demonstrates the energy per mass and per volume for various types of thermite systems compared to TNT, PETN, and RDX, which are some of the most powerful traditional energetic materials. The thermite formulations have much higher energy capacity per volume, compared to traditional energetic materials. However, this large energy capacity can only be utilized, if the thermites are at nano-scale. When reducing the thermite reactants particle size to nano-sized domain, the contact between reagents particles becomes much more intimate than in micron-sized particles, and size reduction decreases the diffusion and transport limitations (Grainer (2004), Pantoya (2006), Bouma et al (2007), Johnson et al (2007), Wang et al (2007),

Comet et al (2010). Thus, the successful energy utilization in nano-thermite mixtures gives them great potential to become the next generation explosives both in military (explosives, propellants, primers, pyrotechnics) and civilian applications (energy, mining, etc) (Martirosyan (2011), Mizolek (2002), Puszynski (2009), Rogachev et al (2010).

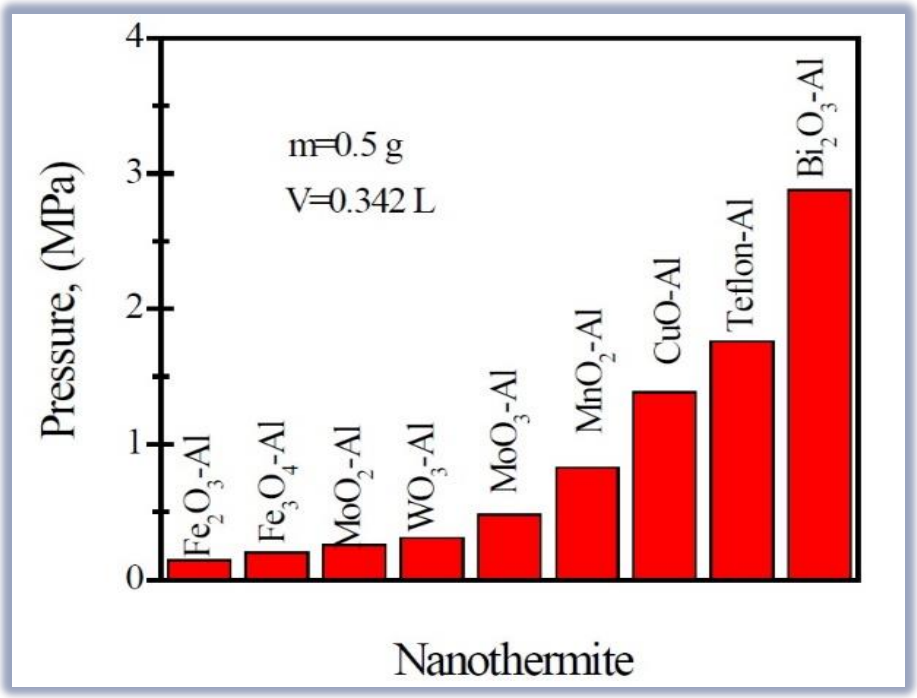

Figure 1-2. The values of the peak pressure obtained during the explosion of different nanoenergetic thermite formulations. The mass of the samples was 0.5 g, and the reactor volume of 0.342 L. (Copyright -Martirosyan (2011), used by permission).

We should note that the energy capacity has critical role in determining the pressure discharge capability of energetic materials. The experimental pressure discharge determination for various nano-thermites is presented in Figure 1-2. The composition Al-Bi_2O_3 performed significantly better (5.6 MPa/g) compared to other systems. The Al-I2O5 system has even higher

pressure discharge capability (43.4 MPa/g), as shown in (Hobosyan and Martirosyan, 2017). As discussed in Figure 1-1, bismuth and iodine oxides mixtures with aluminum, have one of the highest energetic capacities per volume, among common nano-thermite systems.

Although much research has been performed to investigate the properties of metal oxide based on the nano thermites, another closely related systems based on metal hydroxides were surprisingly overlooked. However, these systems undoubtedly deserve attention for several reasons. For example, thermodynamic calculations (performed below) show that energetic capacity per mass for Al-$Bi(OH)_3$ is close to Al-Bi_2O_3. This offers a strong indication that this system can generate sufficient pressure discharge and overtake almost all known nano thermites. Furthermore, most of the methods for production of bismuth trioxide particles utilize sol-gel methods, where the final product usually contains significant amounts of $Bi(OH)_3$ remnants. Thus, it is important to estimate the impact that these remnants can have on Al-Bi_2O_3 nano-thermite. Finally, it was estimated that the Al-$Bi(OH)_3$ discharge generates twice more gas amount per gram of initial thermite mass, when compared to gases generated in the system Al-Bi_2O_3 (Hobosyan et al, 2016). Thermodynamic calculations (shown below) reveal that aluminum-hydroxide systems are in fact just as energetic as aluminum-oxide systems, and generally produce more gas. Because of these features of aluminum-hydroxide nano-thermite systems, it is possible that these systems would perform better for militaristic explosive applications, rocket propulsion, and other situations were instantaneous release of copious amounts of hot gas is desired. Therefore, in the applications where the utilization of gas generation with lower average molecular weight is more important, then systems based on metal hydroxides can be superior to oxides based thermites.

CHAPTER II

THERMODYNAMIC ANALYSIS AND DISCHARGE PRESSURE TESTING OF HYDROXIDE-BASED NANO-THERMITES

2.1. Introduction

In a recent study (Hobosyan et al, 2016), it was stated that nano-thermites oxides have been studied extensively (Nellums et al (2013), Kevin et al (2007), Zhou et al (2014), Baijot et al (2015) while hydroxide type of oxidizers have not yet been investigated. Thermodynamic calculations (shown below) reveal that aluminum-hydroxide systems are in fact just as energetic as aluminum-oxide systems, and generally produce more gaseous phases. Because of these features of aluminum-hydroxide nano-thermite systems, it is possible that these systems would be superior for gas generators applications, rocket propulsion, safety airbags, and other situations were instantaneous release of copious amounts of hot gas is desired.

In this chapter, we investigate 22 nano-thermite systems. Each system is subjected to thorough thermodynamic analysis. Aluminum-oxide systems have been examined and studied extensively, throughout literature, therefore we will not cover them in this work.

The Aluminum-oxide systems which have been examined and studied extensively are presented in (Patel et al (2015), Cheng et al (2010), Demitros et al (2008).

2.2. Thermodynamic analysis background

The thermodynamic estimation of the equilibrium composition of multicomponent multiphase systems requires minimization of the thermodynamic free energy (G) subject to mass and energy balances (Greiner et al, 1995). The thermodynamic calculations were made using "Thermo" software (Shiryaev, 1995), which includes database with thermochemical properties of approximately 3000 compounds. We used additionally the thermo-chemical computer code HSC Chemistry-7 for prediction of the adiabatic temperature and equilibrium compositions. Input and output species, as well as their amounts and initial temperatures, were defined for the calculations of adiabatic temperature and equilibrium concentrations. Theoretical heat balances were calculated by taking molecular amounts of species from the reaction equations and equilibrium calculations. HSC Chemistry-7 includes database of over 25000 compounds.

The composition of the equilibrium products and adiabatic temperature can be determined by minimizing the thermodynamic potential. For a system with N(g) gas and N(s) solid number of components, at constant pressure, the concentrations of equilibrium phases can be expressed as:

$$F(\{n_k\},\{n_s\}) = \sum_{k=1}^{N(g)} n_k \left(ln \frac{p_k}{p} + G_k \right) + \sum_{l=1}^{N(s)} n_l G_l \qquad (2\text{-}1)$$

Where p_k is the partial pressure of the k`th gas-phase component, while n_l and G_l are the number of moles and molar Gibbs free energy of components. The adiabatic combustion temperature, T_c^{ad}, is determined by total energy balance:

$$\sum_{i=1}^{N_0} H_i(T_0) = \sum_{k=1}^{N(g)} n_k H_k(T_c^{ad}) + \sum_{l=1}^{N(s)} n_l H_l(T_c^{ad}) \qquad (2\text{-}2)$$

Where the enthalpy of each component is

$$H_i(T) = \Delta H^0_{f,i} + \int_{T_0}^{T} c_{p,i} dT + \sum \Delta H_{s,i} \qquad (2\text{-}3)$$

and $\Delta H^0_{f,i}$ is the heat of formation at 1 atm and reference temperature T_0, $c_{p,i}$ is the heat capacity, and $\Delta H_{s,i}$ is the heat of s`th phase transition for components (Varma et al, 1998). The combination of both above mentioned software programs made it possible to estimate the equilibrium composition, adiabatic temperature, gas generation, and standard enthalpy of formation for each examined system.

2.3. Thermodynamic analysis results

Table 2-1 is presenting the thermite systems at stoichiometric composition, the adiabatic temperature, gas generation and the reaction enthalpy for these formulations. The detailed calculations and discussions are provided below for each system. Figure 2-1 demonstrates the gas generation per mass of thermite for the formulations analyzed in table 2-1. The lowest gas generation 1-1.3 L/g was observed for rare-earth hydroxide based thermites (except of cerium hydroxide based thermite). Most of the hydroxide based thermites showed large gas generation of over 2 L/g.

Hydroxides				
Combustion Systems	**Maximum adiabatic combustion temperature (K)**	**Gas Production** grams of gas per gram	**Enthalpy ΔH°**	
			kJ/g	kJ/cc
2 Al + $Bi(OH)_3$	3001	0.685	-3.06	-13.34
5 Al + 3 $Ce(OH)_4$	2807	0.036	-3.34	-50.66
4 Al + 3 $Co(OH)_2$	2815	0.107	-4.48	-14.80
2 Al + $Co(OH)_3$	2855	0.220	-5.77	-19.90
4 Al + 3 $Cr(OH)_2$	2448	0.042	-3.76	-34.37
2 Al + $Cr(OH)_3$	2578	0.081	-4.46	-35.00
5 Al + 4 $Cu(OH)_2$	2607	0.349	-4.82	-15.24
Al + $Fe(OH)_2$	2739	0.084	-3.51	-11.24
2 Al + $Fe(OH)_3$	2843	0.146	-5.26	-15.66
Al + $Gd(OH)_3$	1771	0.013	-1.10	-25.93
10 Al + 9 HIO	2040	0.875	-1.66	-26.01
5 Al + 3 HIO_3	3727	0.682	-5.47	-22.10
Al + $Ho(OH)_3$	2215	0.012	-1.39	33.87
2 Al + $In(OH)_3$	2309	0.536	-3.46	-13.21
Al + $La(OH)_3$	2119	0.014	-1.49	-32.28
5 Al + 7 $Mn(OH)_2$	2049	0.091	-2.12	-6.66
8 Al + 3 $MoO_3 \cdot H_2O$	3556	0.053	-4.97	-43.58
Al + $Nd(OH)_3$	2092	0.014	-1.48	-32.90
5 Al + 4 $Ni(OH)_2$	2679	0.111	-4.35	-15.66
2 Al + $Ni(OH)_3$	3297*	0.439	-6.09	-49.87
Al + $Sm(OH)_3$	2186	0.013	-1.53	-35.06
2 Al + $WO_3 \cdot H_2O$	3420*	0.687	-2.60	-39.48

* Calculated by THERMO

Table 2-1. Calculated maximum adiabatic combustion temperature, gas production and enthalpy of reactions of several aluminum hydroxides systems.

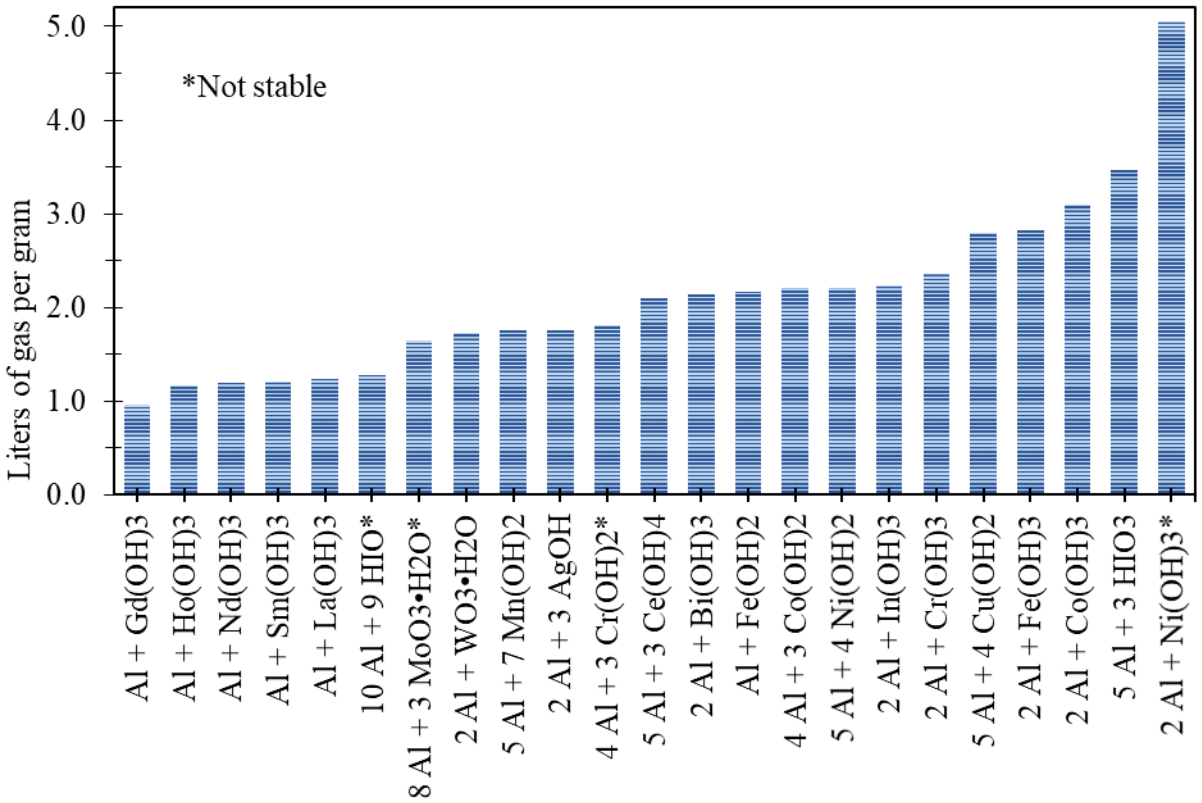

Figure 2-1. Gas generation amount of several aluminum - hydroxide compositions at maximum combustion temperature.

The Al-$Cr(OH)_2$ system shown in Figure 2-2a is exothermic. There is a moderate amount of gas generated per gram at maximum temperature. The temperature increases sharply between 0.1 and 0.3 moles. During this period $Cr(OH)_2$ reacts with the aluminum to form solid chromium, solid aluminum oxide and hydrogen gas. Between 0.3 and 0.5 moles the temperature is stable as the solid chromium melts in increasing amounts and aluminum is fast transformed into gaseous compounds. With additions of oxidizer, there is a gradual increase of temperature up to the peak temperature of 2448 K at 0.75 moles. After this point hydrogen continues to form in linearly increasing amounts and the energy of the system is being used in forming a little

water vapor, a linearly increasing amount of solid chromia, and liquid chromium. Thus, the temperature very gradually decreases from 0.75 to 1.6 moles.

Al-$Cr(OH)_3$ system shown in Figure 2-2b is exothermic. There is a large amount of gas generated per gram at maximum temperature. The temperature increases between 0.1 and 0.2 moles. During this period $Cr(OH)_3$ reacts with the aluminum to form solid chromium, solid aluminum oxide, hydrogen gas, and $Al_2O(g)$. Between 0.2 and 0.3 moles the temperature plateaus as the solid chromium melts in increasing amounts. Between 0.3 and 0.5 moles the aluminum oxide is formed in liquid form as the temperature rises above its melting point. At 0.5 moles the temperature peaks at 2578 K. After this point hydrogen continues to increase linearly and the energy of the system is being used in forming a little water vapor, a linearly increasing amount of solid chromia, and liquid chromium. Thus, the temperature very gradually decreases from 0.5 to 1.0 mole.

The Al-MoO_3•H_2O system shown in Figure 2-2c is highly exothermic. There is a moderate amount of gas released per gram at maximum temperature. From 0.1 to 0.2 moles the temperature is stable as aluminum reacts with increasing amounts of oxidizer and produces less liquid aluminum. From 0.2 to 0.4 moles the temperature increases rapidly due to a sufficient amount of oxidizer to react with aluminum to produce mostly stoichiometric equation products. At 0.4 moles the temperature is maximized to 3556 K. From 0.4 to 1.0 mole there is an increasing excess of oxidizer, which causes the temperature to decrease.

The Al-WO_3•H_2O system shown in Figure 2-2d is highly exothermic. There is a moderate amount of gas emitted per gram at maximum temperature. From 0.1 to 0.3 moles the temperature increases slowly as oxidizer is added to the system in increasing amounts and almost all the reactants are being fast transformed into gaseous compounds. A notable dip occurs

between 0.2 and 0.3 moles where aluminum oxide is formed in both solid and liquid form. From 0.3 to 0.5 moles the temperature increases rapidly with the addition of oxidizer. At 0.5 moles the temperature peaks to 3420 K where the system is in stoichiometric equilibrium. From 0.5 to 1.0 mole the temperature steadily decreases as excess amounts of oxidizer are introduced into the system. A notable slowing in the decreasing of the temperature occurs between 0.8 and 0.9 moles where aluminum oxide is formed in both the liquid and solid phases.

The Al-$Fe(OH)_2$ system displayed in Figure 2-3a is exothermic. There is a large amount of gas generated per gram at maximum temperature. The temperature increases rapidly between 0.1 and 0.3 moles as increasing amounts of oxidizer are added to the system. The temperature plateaus from 0.3 to 0.5 moles as aluminum is fast transformed into increasing amounts of gaseous compounds. After 0.5 moles the heat energy is sufficient to fast transform iron into the gaseous phase, and also to form mostly stoichiometric equation products. The temperature increases up until 0.75 moles at which point the temperature peaks at 2739 K. Saturation of oxidizer occurs after this point, which leads to a decrease in temperature from 0.75 to 1.1 moles. From 1.1 to 1.2 moles there is stability in temperature coinciding with the production of aluminum oxide in both the solid and liquid phases. After this transition period the temperature continues to decrease until 1.5 moles. From 1.5 moles to 1.6 moles the temperature stabilizes again as Al_2FeO_4(s) begins to form rather than solid aluminum oxide and FeO(l).

The Al-$Fe(OH)_3$ system presented in Figure 2-3b is exothermic. There is a large amount of gas generated per gram at maximum temperature. Between 0.1 and 0.2 moles the temperature increases as oxidizer is added in greater amounts. Temperature stabilizes between 0.2 and 0.3 moles in congruence with the fast transform of aluminum into gaseous compounds in increasing amounts. After 0.3 moles there is a sufficient amount of heat energy to generate mostly

stoichiometric equation products. Temperature continues to increase up to 0.5 moles at which the oxidizer and fuel are in stoichiometric equilibrium and the temperature peaks to 2843 K. After 0.5 moles the temperature decreases as excess amounts of oxidizer are added to the system. The temperature decreases more slowly from 0.8 to 1.0 mole. In this area there is transition period where the formation of aluminum oxide happens in both the solid and liquid states.

The Al-$Co(OH)_2$ system shown in Figure 2-3c is exothermic. There is a large amount of gas generated per gram at maximum temperature. The temperature increases between 0.1 and 0.4 moles in congruence with a decreasing amount of liquid aluminum. During this period the aluminum reacts to form multiple products. Among these products are multiple fast transformed gases, which cause the plateau in temperature around 0.3 moles. As more fuel is added to the system, the temperature gradually increases between 0.4 and 0.75 moles where it peaks at 2815 K. Further addition of oxidizer to the system results in products composed solely from $Co(OH)_2$. Notably there was initially no water vapor as a product, just hydrogen gas. Because of the increased amount of oxygen from the $Co(OH)_2$ and lack of aluminum for it to oxidize (after 0.75 moles), hydroxides are ripped from the oxidizer to form water vapor. Between 1.2 and 1.4 moles the temperature temporarily plateaus at the freezing point of aluminum oxide. After this point, the aluminum oxide is formed in the solid state, and temperature continues to decrease until 1.6 moles.

The Al-$Co(OH)_3$ system shown in Figure 2-3d is exothermic. There is a copious amount of gas generated per gram at maximum temperature. Temperature increases from 0.1 to 0.2 moles after which point there is sufficient oxidizer to react virtually completely with all present aluminum. From 0.2 to 0.3 moles the temperature increases rapidly with increasing presence of oxidizer. Between 0.3 and 0.4 moles there is a plateau in temperature where aluminum is being

fast transformed into gaseous compounds. After 0.4 moles temperature increases up until 0.5 moles where the temperature peaks at 2855 K when the system is in stoichiometric equilibrium. Temperature decreases steadily from 0.5 to 2.0 moles with two brief periods of stability. One period occurs between 1.1 and 1.3 moles where aluminum oxide is formed in both the liquid and solid phases. The other occurs between 1.5 and 1.7 moles where cobalt oxide is formed in both liquid and solid phases.

The Al-Ni$(OH)_2$ system shown in Figure 2-4a is exothermic. There is a large amount of gas generated per gram at maximum temperature. Temperature increases from 0.1 to 0.2 moles with addition of oxidizer to the system. From 0.2 to 0.3 moles there is a brief plateau in temperature due to the fast transform of aluminum into gaseous compounds. Temperature continues to increase from 0.3 to 0.4 moles. Between 0.4 and 0.7 temperature once again plateaus. During this period the majority of the nickel is being formed into AlNi(l) and Ni(l). After this transition period the temperature briefly increases from 0.7 to 0.8 moles where the temperature peaks to 2679 K. Between 0.8 and 1.3 moles the temperature decreases with excess of oxidizer. From 1.3 to 1.4 moles there is a brief plateau due to the formation of aluminum oxide in both the liquid and solid states. Temperature continues to decrease from 1.4 to 2.0 moles with ever increasing excessive amounts of oxidizer.

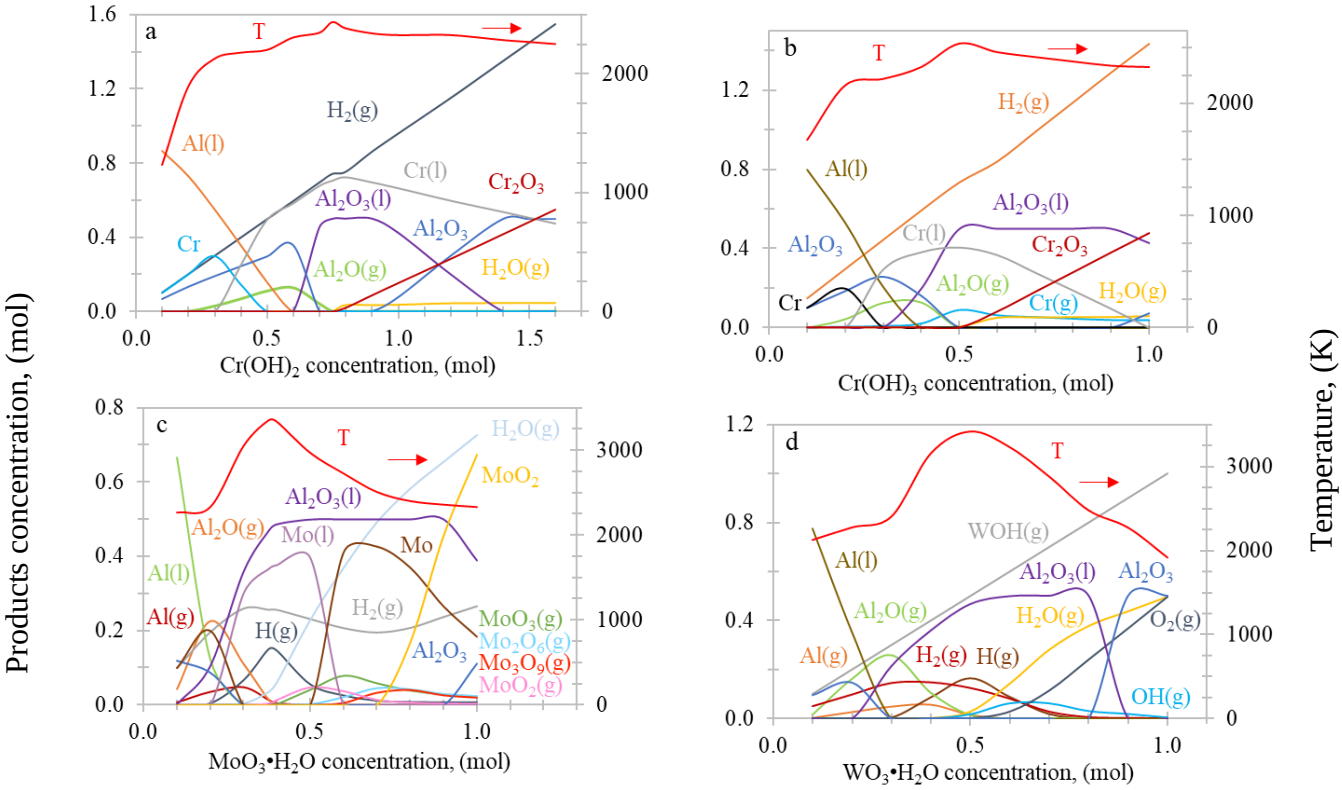

Figure 2-2. Dependence of the adiabatic temperature and equilibrium concentrations of solid, liquid, and gaseous phases during exothermic reaction of transition metals (Group 6) hydroxides with aluminum: (a) Al-$Cr(OH)_2$; (b) Al-$Cr(OH)_3$; (c) Al-MoO_3•H_2O; and (d) Al-WO_3•H_2O systems (red line labeled with T represents adiabatic combustion temperature).

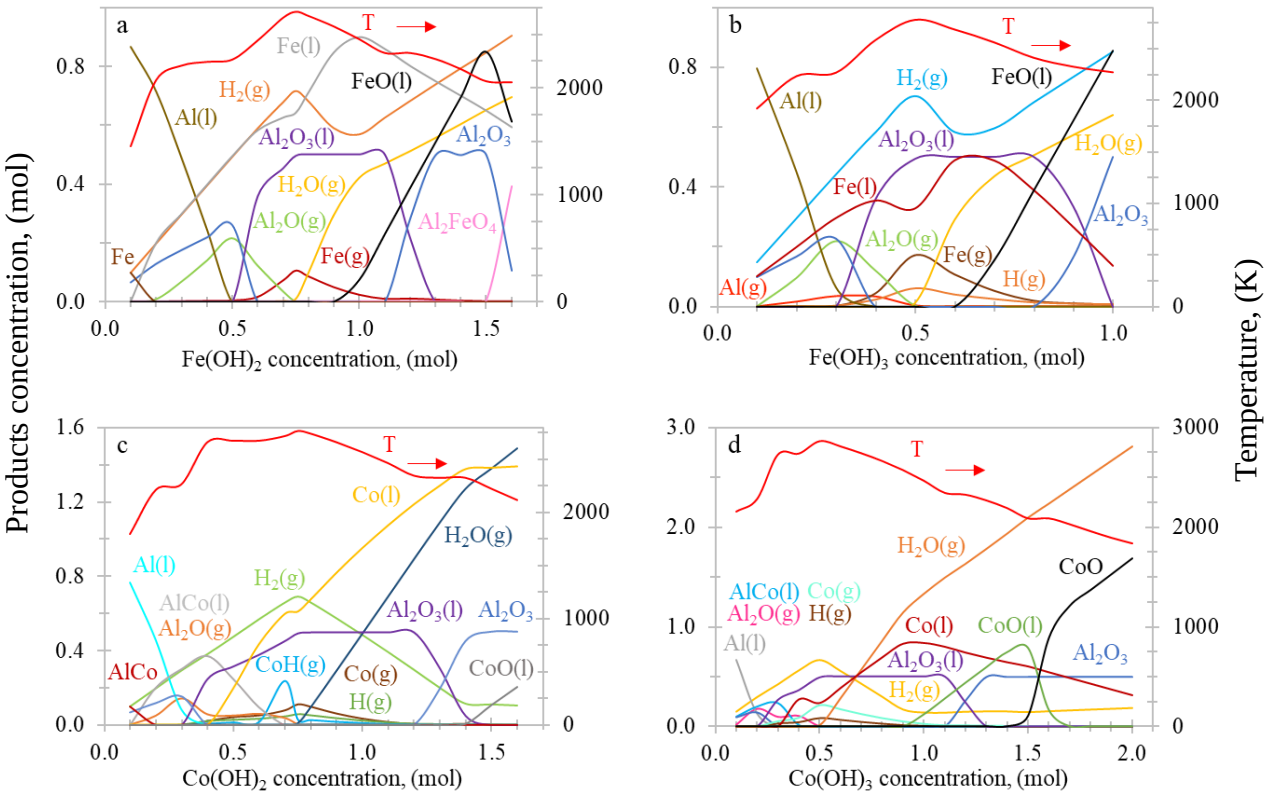

Figure 2-3. Dependence of the adiabatic temperature and equilibrium concentration of solid, liquid, and gaseous phases during exothermic reaction of transition metals (Groups 8, 9) hydroxides with aluminum: (a) Al-$Fe(OH)_2$; (b) Al-$Fe(OH)_3$; (c) Al-$Co(OH)_2$; and (d) Al-$Co(OH)_3$ systems (red line labeled with T represents adiabatic combustion temperature).

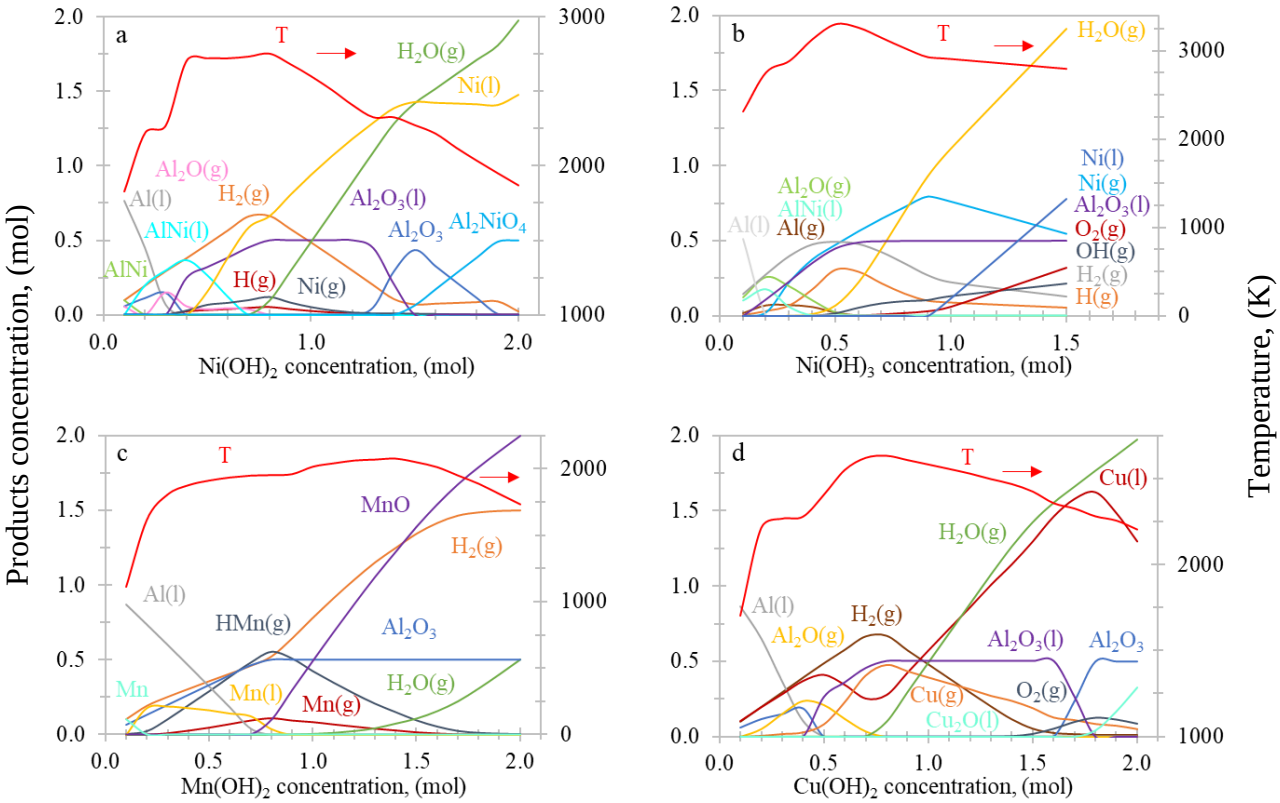

Figure 2-4. Dependence of the adiabatic temperature and equilibrium concentration of solid, liquid, and gaseous phases during exothermic reaction of transition metals (Groups 7, 10, 11) hydroxides with aluminum: (a) Al-$Ni(OH)_2$; (b) Al-$Ni(OH)_3$; (c) Al-$Mn(OH)_2$; and (d) Al-$Cu(OH)_2$ systems (red line labeled with T represents adiabatic combustion temperature).

The Al-$Ni(OH)_3$ system shown in Figure 2-4b is highly exothermic. This system produces the most gas per gram at maximum temperature. Temperature increases rapidly from 0.1 to 0.2 moles, then more slowly from 0.2 to 0.3 moles, and then continues to increase rapidly from 0.3 to 0.5 moles. The slowing in temperature gain between 0.2 and 0.3 moles is caused by the fast transform of aluminum into gaseous forms. This slowing area is quickly overcome with the addition of oxidizer to the system. At 0.5 moles the system is in stoichiometric equilibrium and the temperature is maximized to 3297 K*. From 0.5 to 0.8 moles there is an excess of oxidizer leading the temperature to decrease. From 0.8 to 1.5 moles the temperature decreases more slowly in congruence with the formation of nickel in both the gaseous and solid phases.

The Al-$Mn(OH)_2$ system shown in Figure 3-4c is exothermic. There is a moderate amount of gas generated per gram at maximum temperature. From 0.1 to 0.3 moles there is a sharp increase in temperature with addition of oxidizer to the system. Between 0.3 and 0.9 moles there is a stability in temperature due to the fast transform of constituents into gaseous compounds. After 0.9 moles there is sufficient oxidizer to gradually increase the temperature. Temperature increases until 1.4 moles at which point the system is in stoichiometric equilibrium and the temperature is maximized to 2049 K After 1.4 moles, excess in oxidizer lead to a decrease in temperature to 2.0 moles.

The Al-$Cu(OH)_2$ system shown in Figure 2-4d is exothermic. It produces a large amount of gas per gram at maximum temperature. From 0.1 to 0.2 moles the temperature increases rapidly with the increase of oxidizer. Between 0.2 to 0.4 moles there is a plateau in temperature due to the fast transform of aluminum into gaseous compounds. After 0.4 moles there is sufficient oxide to react virtually completely with available aluminum. Temperature begins to increase once again and continues to increase until the system is in stoichiometric equilibrium at

0.8 moles where the temperature peaks to 2607 K. From 0.8 to 2.0 moles the temperature decreases with excess amounts of oxidizer.

The Al-$Bi(OH)_3$ system shown in Figure 2-5a is highly exothermic. There is a large amount of gas produced per gram at maximum temperature. Temperature increases from 0.1 to 0.2 moles with increasing amount of oxidizer added to the system. From 0.2 to 0.3 moles there is a plateau in temperature due to the fast transform of aluminum into gaseous forms. After 0.3 moles there is sufficient oxidizer to react almost completely with aluminum and the temperature begins to increase again with increased amounts of oxidizer. Temperature increases up until 0.5 moles at which point the temperature peaks to 3001 K. After 0.5 moles excess of oxidizer leads the temperature to decrease. Between 0.8 and 1.0 mole, aluminum oxide is formed in both the liquid and solid phase. This transitionary period occurs in congruence with a stability in the temperature. From 1.0 mole to 1.2 moles the temperature continues to decrease due to excess oxidizer.

The Al-$In(OH)_3$ system shown in Figure 2-5b is exothermic. There is a large amount of gas generated per gram at maximum temperature. Temperature increases between 0.1 and 0.2 moles with increase of oxidizer. From 0.2 to 0.4 moles the temperature plateaus due to the fast transform of aluminum into gaseous compounds. Between 0.4 and 0.5 moles there is sufficient oxidizer to react with virtually all available aluminum and temperature increases. At 0.5 moles the temperature peaks to 2309 K due to the system falling into stoichiometric equilibrium. After 0.5 moles there is excess in oxidizer. This excess leads the temperature to decrease continuously from 0.5 to 1.0 mole.

The Al-HIO system shown in Figure 3-5c is exothermic. There is a moderate amount of gas generated per gram at maximum temperature. Temperature increases from 0.1 to 0.6 moles

as increasing amounts of oxidizer react with fuel. From 0.6 to 0.8 moles the temperature increases more rapidly as nearly all the elemental aluminum reacts to form other compounds. Temperature stabilizes between 0.8 and 1.0 mole with the peak temperature of 2040 K being at 0.9 moles. After this stabilization period where oxidizer and fuel are being fast transformed into various gaseous compounds, the temperature begins to decrease. It decreases from 1.0 to 1.5 moles and then more rapidly from 1.5 to 1.8 moles once all the aluminum reacts with HIO to become aluminum oxide.

The Al-HIO_3 system shown in Figure 2-5d is highly exothermic. There is a copious amount of gas generated per gram at maximum temperature. Temperature increases from 0.1 to 0.3 moles with increased amounts of oxidizer. The temperature rises more slowly from 0.3 to 0.5 moles as the oxidizer and fuel are fast transformed into multiple gaseous compounds. At 0.5 moles the temperature peaks to 3727 K after which the temperature decreases with the addition of oxidizer. This decreases in temperature continues from 0.5 to 1.0 mole with the greater saturation of oxidizer.

The Al-$La(OH)_3$ system shown in Figure 2-6a is exothermic. There is a moderate amount of gas generated per gram at maximum temperature. Temperature increases between 0.1 and 0.2 moles with addition of oxidizer. From 0.2 to 0.4 moles the temperature plateaus. During this point there is not sufficient oxidizer to provide enough energy to dissociate the Al2La(s) that forms. After 0.4 moles there is sufficient energy and the temperature of the system increases leading up to the maximum temperature of 2119 K at 1.0 mole where the system is in stoichiometric equilibrium. From 1.0 to 2.0 moles there is excess of oxidizer, which causes the temperature to decrease.

The Al-$Ce(OH)_4$ system shown in Figure 2-6b is exothermic. There is a large amount of gas generated per gram at maximum temperature. Temperature increases from 0.1 to 0.2 moles. A brief plateau occurs between 0.2 and 0.4 moles due to the fast transform of aluminum into gaseous forms. After 0.4 moles there is sufficient oxidizer to react virtually completely with all available aluminum and temperature increases once again. Temperature increases all the way up to 0.6 moles at which point the system is in stoichiometric equilibrium and the temperature is maximized to 2807 K. From 0.6 to 0.8 moles the temperature decreases with excess of oxidizer. From 0.8 to 1.0 mole there is a stability in temperature where cerium(III) oxide is being formed in both liquid and solid phases.

The Al-$Nd(OH)_3$ system shown in Figure 2-6c is exothermic. There is a moderate amount of gas generated per gram at maximum temperature. Temperature increases from 0.1 to 1.0 mole with addition of oxidizer. At 1.0 mole the system is in stoichiometric equilibrium and the temperature is maximized to 2092 K. From 1.0 to 2.0 moles there is an excess of oxidizer, which is the cause for the temperature of the system to decrease.

The Al-$Sm(OH)_3$ system shown in Figure 3-6d is exothermic. There is a moderate amount of gas generated per gram at maximum temperature. Temperature increases from 0.1 to 1.0 mole with increasing amounts of oxidizer. At 1.0 mole the system is in stoichiometric equilibrium and the temperature is maximized to 2186 K. From 1.0 to 2.0 moles there is excess oxidizer in the system, which is the cause for the temperature to decrease.

The Al-$Gd(OH)_3$ system shown in Figure 2-6e is moderately exothermic. There is a small amount of gas generated per gram at maximum temperature. The system as a whole is composed of sublinear changes in amounts of products. Temperature increases between 0.1 to 1.0 mole at

which point the temperature peaks at 1771 K. From 1.0 to 2.0 moles there is an excess of oxidizer, which causes the temperature to decrease.

The Al-Ho$(OH)_3$ system shown in Figure 2-6f is exothermic. There is a moderate amount of gas generated per gram at maximum temperature. Temperature increases from 0.1 to 1.0 mole with increased amounts of oxidizer. At 1.0 mole the temperature peaks to 2215 K after which the temperature decreases with the addition of oxidizer. This decreases in temperature continues from 1.0 to 2.0 moles due to the saturation of oxidizer.

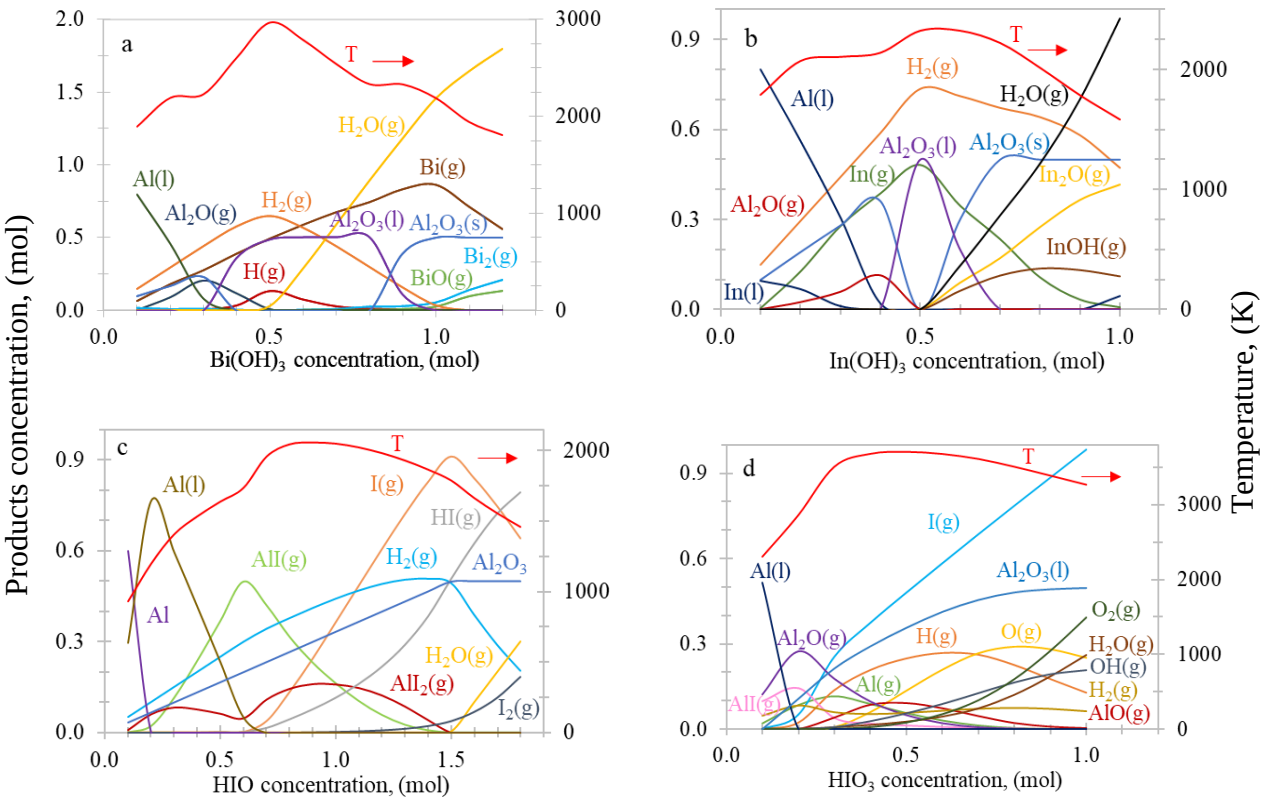

Figure 2-5. Dependence of the adiabatic temperature and equilibrium concentration of solid, liquid, and gaseous phases during exothermic reaction of bismuth, indium and iodine compounds with aluminum (a) Al-$Bi(OH)_3$; (b) Al-$In(OH)_3$; (c) Al-HIO; and (d) Al-HIO_3 systems (red line labeled with T represents adiabatic combustion temperature).

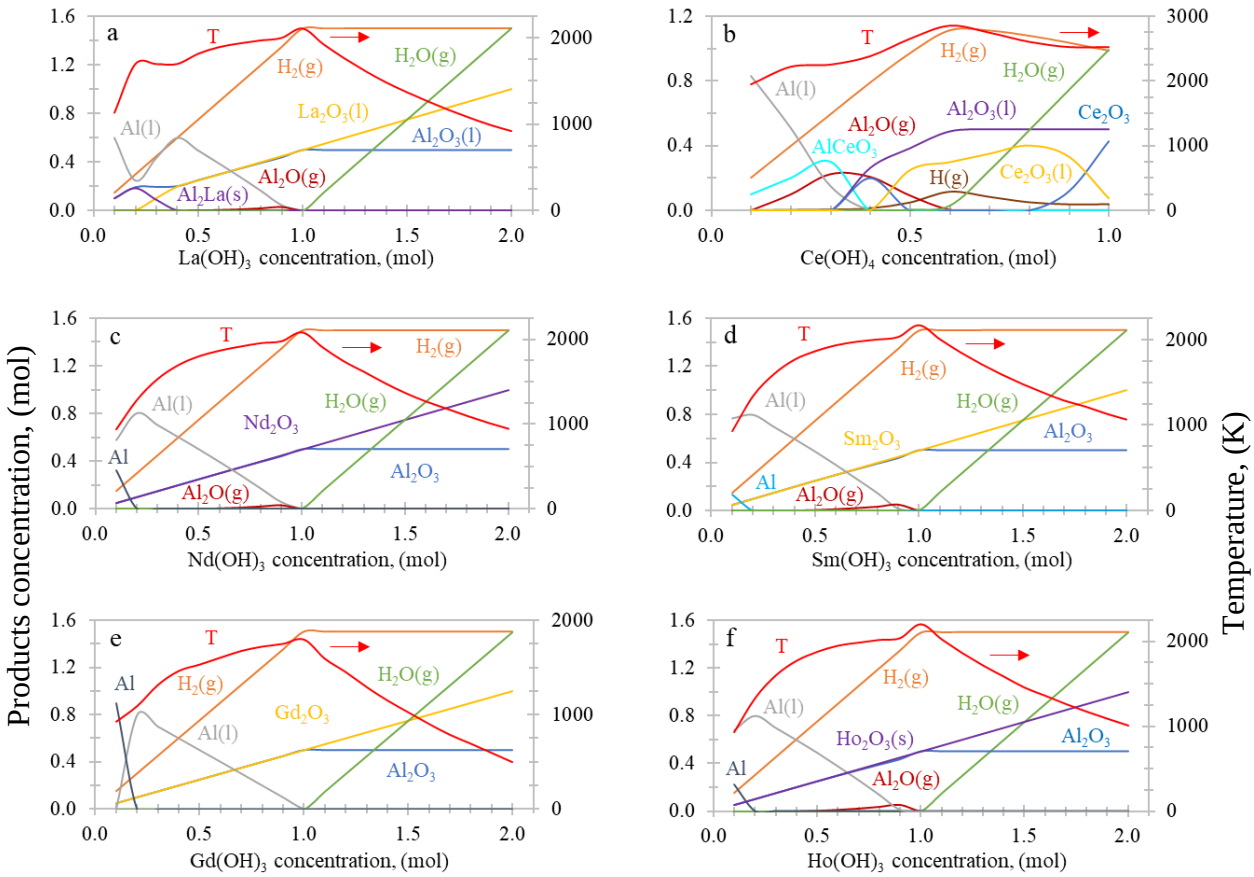

Figure 2-6: Dependence of the adiabatic temperature and equilibrium concentration of solid, liquid, and gaseous phases during exothermic reaction of rare earth metal hydroxides with aluminum: (a) Al-La(OH)$_3$; (b) Al-Ce(OH)$_4$; (c) Al-Nd(OH)$_3$; (d) Al-Sm(OH)$_3$; (e) Al-Gd(OH)$_3$; and (f) Al-Ho(OH)$_3$ systems (red line labeled with T represents adiabatic combustion temperature

2.4. Preparation and Testing of Nano-thermites

In order to show the practical application of thermodynamic calculations, 4 above discussed systems were chosen to prepare hydroxide based nano-thermite formulations Al-

$Bi(OH)_3$, Al-$Cu(OH)_2$, Al-$Ce(OH)_4$ and Al-$Ni(OH)_2$. As the thermodynamic calculations have shown, the highest temperature was observed close to stoichiometric ratio presented in Table 2-1, which was used to prepare the mixtures of nano-thermites with corresponding weight percentages.

The aluminum nanoparticles (Sigma Aldrich Co) were used for preparation of nanoenergetic formulation and stored under Nitrogen (99.98 %) to avoid any contamination and oxidation. We used aluminum nanoparticles with average size of 100 nm (Figure 2-7a,b). This size, being not very pyrophoric, is covered by approximately 4-5 nm aluminum oxide layer and can be safely mixed with oxidizers under hexane environment in rotary ball mill. The bismuth, copper and nickel hydroxides were purchased from Sigma Aldrich. The aluminum nanoparticles and corresponding hydroxide based oxidizers were mixed in stoichiometric ratios with rotary ball mill in ceramic jar with zirconia balls (5 mm in diameter) for 9 hours, to assure well mixing. After mixing, the powder was dried at 60 ºC under vacuum for 12 hours.

The SEM images of prepared thermite mixtures is presented in Figure 2-7 and Figure 2-8. The Al-Bi(OH)3 mixture at low magnifications (Figure 2-7c) shows mostly uniform distribution of Al nanoparticles in bismuth hydroxide media. The higher magnification (Figure 2-7d) shows that Al nanoparticles are interconnected and are covering the bismuth hydroxide particles.

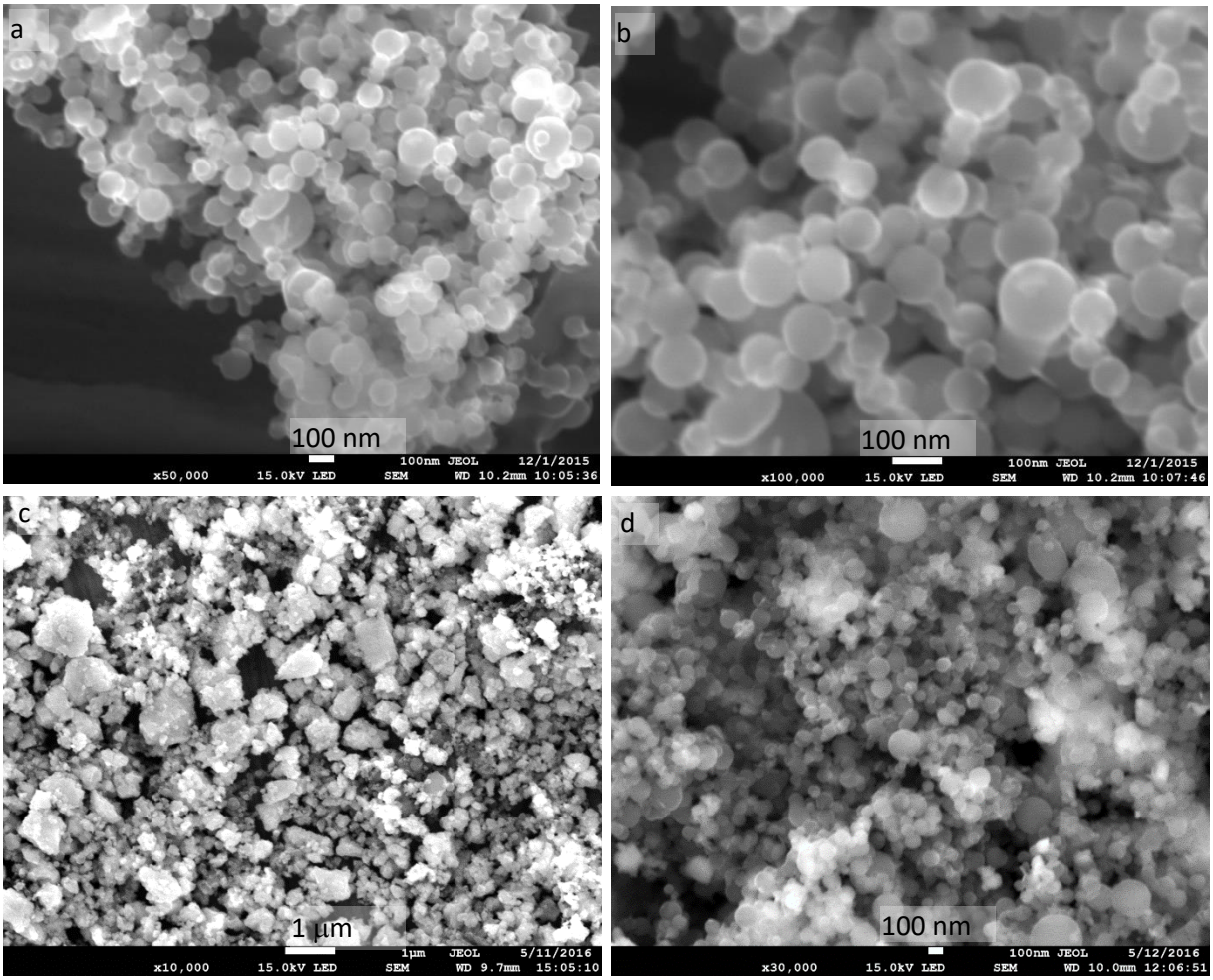

Figure 2-7. SEM of Aluminum nanoparticles at (a) 50 000 and (b) 100 000 times magnification, (c) Al-$Bi(OH)_3$ mixture at 10 000 and (d) 30 000 times magnification

The SEM for Al-$Cu(OH)_2$ mixture shows that the 20-30 μm copper hydroxide particle agglomerates (Figure 2-8a) are covered with Al nanoparticles (Figure 2-8b). In the case of Al-$Ce(OH)_4$ mixture, the inter-connected Al nanoparticles are covering micro-meter sized hydroxide particles (Figure 2-8 c,d). Similarly, for the Al-$Ni(OH)_2$ mixture, the Al nano-particles are covering the micro-meter sized nickel hydroxide particles (Figure 2-8e,f).

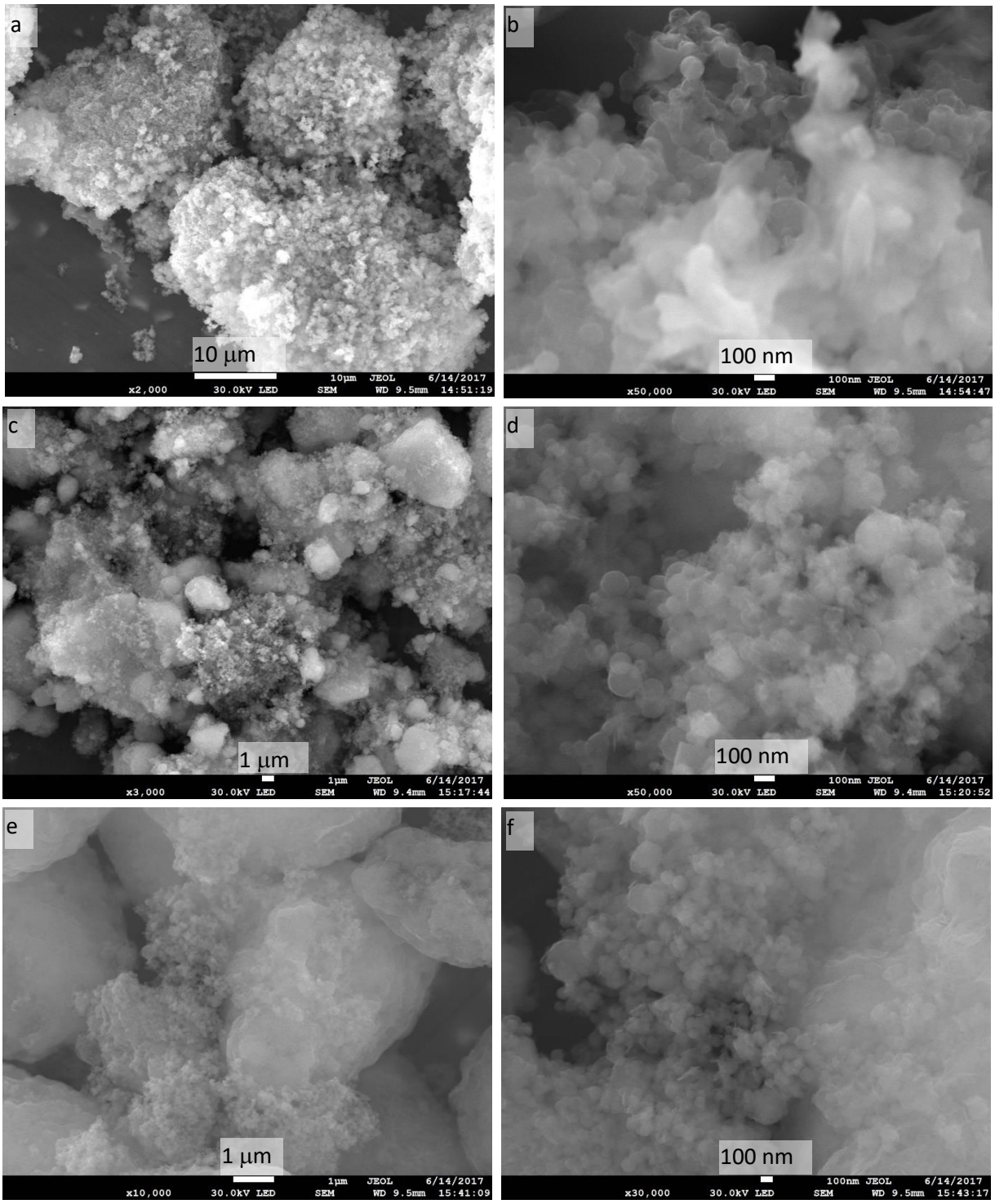

Figure 2-8. SEM images of (a) Al-Cu$(OH)_2$ mixture at 2000 and (b) 50 000 times magnification, (c) Al-Ce$(OH)_4$ mixture at 3000 and (d) 50 000 times magnification, (e) Al-Ni$(OH)_2$ mixture at 10 000 and (f) 30 000 times magnification.

The differential scanning calorimetry (DSC) and thermogravimetric analysis (TGA) of the prepared mixtures was performed using DSC-TGA Q600 (TA Instruments), under nitrogen flow 100 ml/min and heating rate 20 ºC/min.

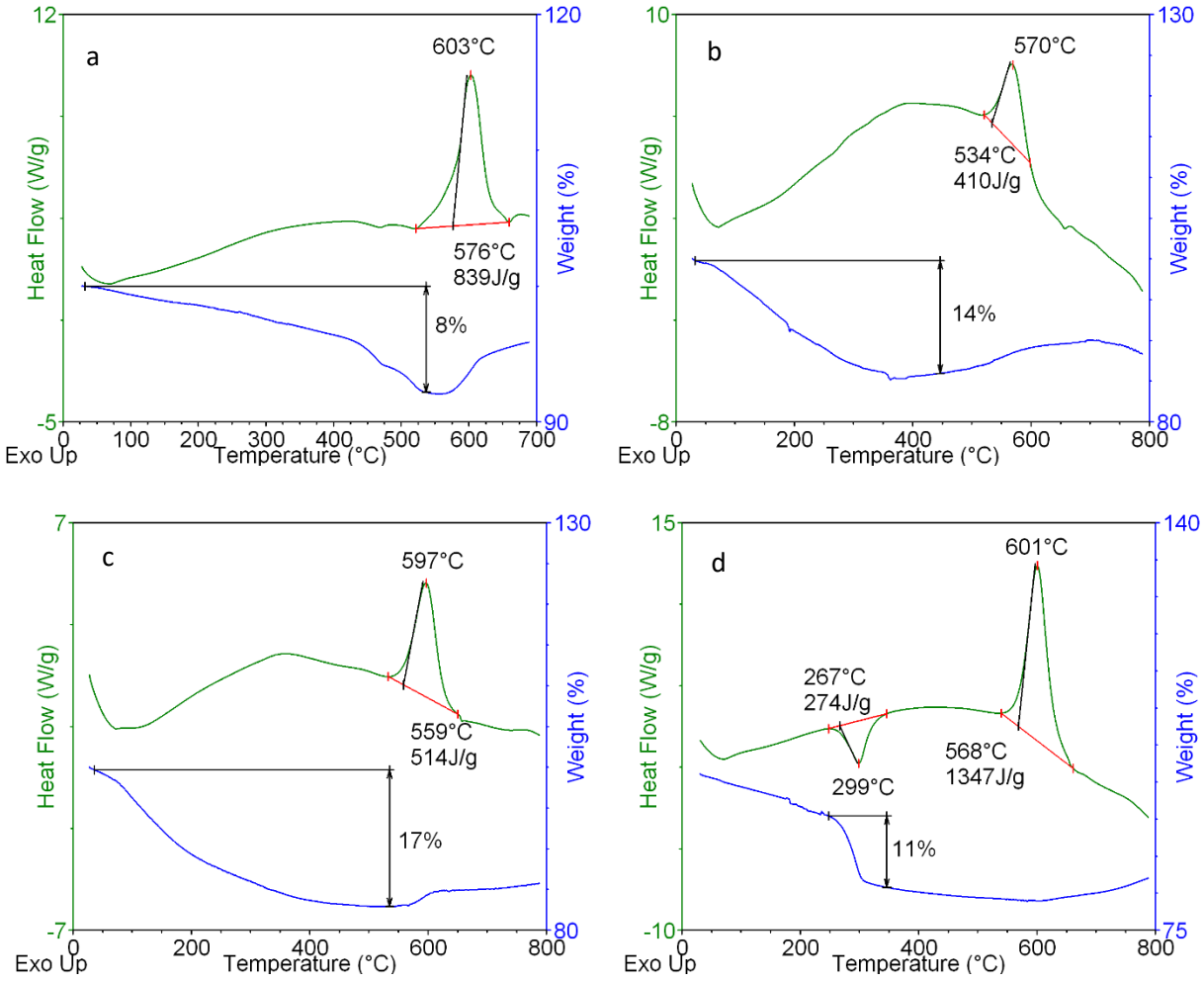

Figure 2-9. Heat flow and weight change dependence on the temperature for: (a) Al–$Bi(OH)_3$ mixture; (b) Al–$Cu(OH)_2$ mixture, (c) Al-$Ce(OH)_4$ mixture, (d) Al-$Ni(OH)_2$ mixture

The results are presented in Figure 2-9. The blue line represents the weight change (wt. %), the green line shows the heat flow (W/g), and the red line indicates the points through which

the heat flow peaks are integrated to estimate the energy released during thermite reaction (J/g). The DSC was pre-calibrated for heat flow curve integration.

The Al-$Bi(OH)_3$ mixture (Figure 2-9a) shows 839 J/g energy release at 603 ºC. Before the exothermic reaction between reagents, the mass decreases by 8 wt. %, indicating that due to slow (20 ºC/min) heating rate, the OH groups partially escaped. We note that the mixture is practically stable until 150 ºC and loses less than 1.5 wt. % mass, which can be attributed to traces of solvents trapped in powder. Similar behavior of exothermic interaction was observed in the system Al-Cu(OH)2 (Figure 2-9b), where 410 J/g energy was released at 570 ºC. The mass decreases by 14 wt. % due to partial escape of OH groups before the reaction. However, this mixture is stable until 100 ºC, thus the Al-$Cu(OH)_2$ mixture can be stored and handled under normal conditions. The analysis results for $Ce(OH)_4$ mixture are presented in Figure 2-9c. This system released energy of 514 J/g at 597 ºC. Similar to previous systems, due to slow heating rate, the weight decreases by 17 wt. % prior to exothermic reaction between constituents, showing partial escape of OH groups. We note that this system is also stable under normal conditions and only less than 2 wt. % decrease was observed below 150 ºC. In the case of Al-$Ni(OH)_2$ mixture, the exothermic interaction was observed at 601 ºC with release of 1347 J/g energy (Figure 2-9d). However, there is an endothermic process at 267 ºC with 274 J/g energy consumption and 11 wt. % mass decrease. This should be attributed to partial decomposition of nickel hydroxide which can occur between 250-340 ºC (Carney et al, 2015). However, the system Al-$Ni(OH)_2$ is stable below 150 ºC. Thus, all four systems exhibited exothermic interaction around 570-600 ºC, which should be considered as the ignition point.

The pressure discharge is an important feature of nano-energetic materials (Martirosyan 2011, Hobosyan et al, 2016). The as-prepared nano-thermite samples with 200 mg mass were

placed into Parr Instrument High Pressure cylindrical reactor with 0.342 L volume. The ignition of the reaction was electrically triggered by Ni-Cr wire, the pressure signals were measured by piezoelectric transducer with rated pressure/voltage values (Omega) and the signals were amplified and recorded trough Omega DAQ-3005 Data Acquisition board with signal acquisition frequency of 1 MHz. The results are presented in Figure 6. Out of four examined systems, the formulation based on bismuth hydroxide showed the highest pressure discharge value of 3.3 MPa in 60 μs timeframe for 200 mg charge (Figure 2-10a).

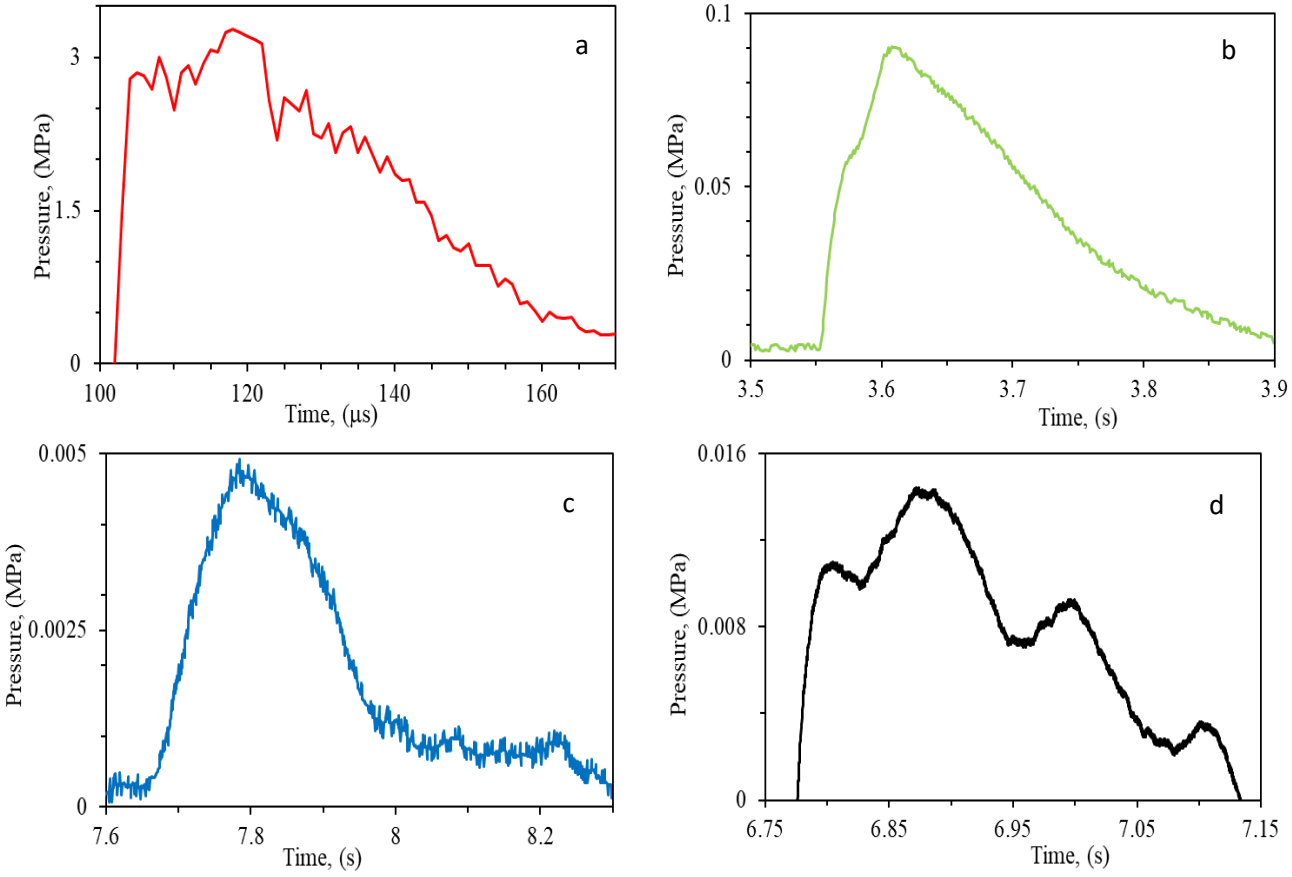

Figure 2-10. Pressure discharge peaks for the systems a) Al-$Bi(OH)_3$, b) Al-$Cu(OH)_2$, (c) Al-$Ce(OH)_4$ and (d) Al-$Ni(OH)_2$, for the thermite charge mass 200 mg in 0.342 L volume

This is a very powerful nano-thermite with one of the highest pressure discharge values reported in literature (Hobosyan et al, 2016), which can be used in high power to mass ratio applications, such as micro-thrusters (Puchades et al, 2017).

The Al-$Cu(OH)_2$ system for the same charge mass generates 0.095 MPa pressure, which is released during 0.3 s timeframe, demonstrating mild thermite characteristics (Figure 3-10b). The Al-$Ce(OH)_4$ system is generating 0.005 MPa pressure discharge for 200 mg charge mass, 0.3 s timeframe (Figure 2-10c), and Al-$Ni(OH)_2$ system generates 0.014 MPa pressure discharge for the same 200 mg mass in timeframe 0.3 s. Both these systems are suitable for applications requiring mild power. The examined systems demonstrate the reliability of thermodynamic calculations to assess the performance of new nano-thermite formulations based on hydroxides.

CHAPTER III

NOVEL NANOENERGETIC SYSTEM BASED ON BISMUTH HYDROXIDE

3.1. Introduction

As we stated in Chapter 2, much research has been performed to investigate the properties of metal oxide based nano thermites, but another closely related systems based on metal hydroxides were surprisingly overlooked. In this chapter, we will have a closer look at the system Al-$Bi(OH)_3$, which undoubtedly deserves more attention for several reasons. First of all, thermodynamic calculations (performed below) show that energetic capacity per mass for Al-$Bi(OH)_3$ is close to Al-Bi_2O_3. This offers a strong indication that this system can generate sufficient pressure discharge and overtake almost all known nano thermites. Furthermore, most of the methods for production of bismuth trioxide particles utilize sol-gel methods, where the final product usually contains significant amounts of $Bi(OH)_3$ remnants. Thus, it is important to estimate the impact that these remnants can have on Al-Bi_2O_3 nano-thermite. Finally, we estimated that the Al-$Bi(OH)_3$ discharge generates twice more gas amount per gram of initial thermite mass, when compared to gases generated in the system Al-Bi_2O_3. Therefore, in the applications where the utilization of gas generation with lower average molecular weight is more important, then systems based on metal hydroxides can be superior to oxides based thermites. In this work, the thermodynamic calculations, as well as pressure discharge dynamics of the system

Al-$Bi(OH)_3$ are investigated for the first time. Moreover, the effect of oxidizer particle through high energy ball milling on the oxidizer decomposition and nano-thermite pressure discharge values are studied and the milling energy and nano-thermite mass-pressure discharge dependences are revealed.

3.2. Thermodynamic Analysis

Thermodynamic analysis of the system Al-$Bi(OH)_3$ are critical to evaluate the energetic capacity of the stoichiometric mixture, prediction of the adiabatic temperature, condensed phase concentrations as well as the amount of gaseous products during the reaction.

The interaction between Al and $Bi(OH)_3$ follows the reaction:

$$2Al + 2Bi(OH)_3 = Al_2O_3 + 2Bi + 3H_2O + \Delta H\ (-1.92\ kJ/g) \qquad (3\text{-}1)$$

According to HSC-7 calculations, the energetic capacity for the system (3-2) is 1.92 kJ/g, which is slightly less than the energetic capacity for the system Al-Bi_2O_3:

$$2Al + Bi_2O_3 = Al_2O_3 + 2Bi + \Delta H\ (-2.12\ kJ/g) \qquad (3\text{-}2)$$

Interesting to note that the energetic density calculated for unit volume for the system (3-1) is 8.83 kJ/cc, while the energetic density for the system (3-2) is 15.2 kJ/cc.

Figure 3-1 shows the dependence of the adiabatic temperature and equilibrium concentration of condensed and gaseous phases during the exothermic reaction in system (3-1). The difference of this figure from Figure 2-5a is that in this case we are changing the amount of aluminum in the system, whereas in calculations in chapter 2 we were changing the amount of oxidizer.

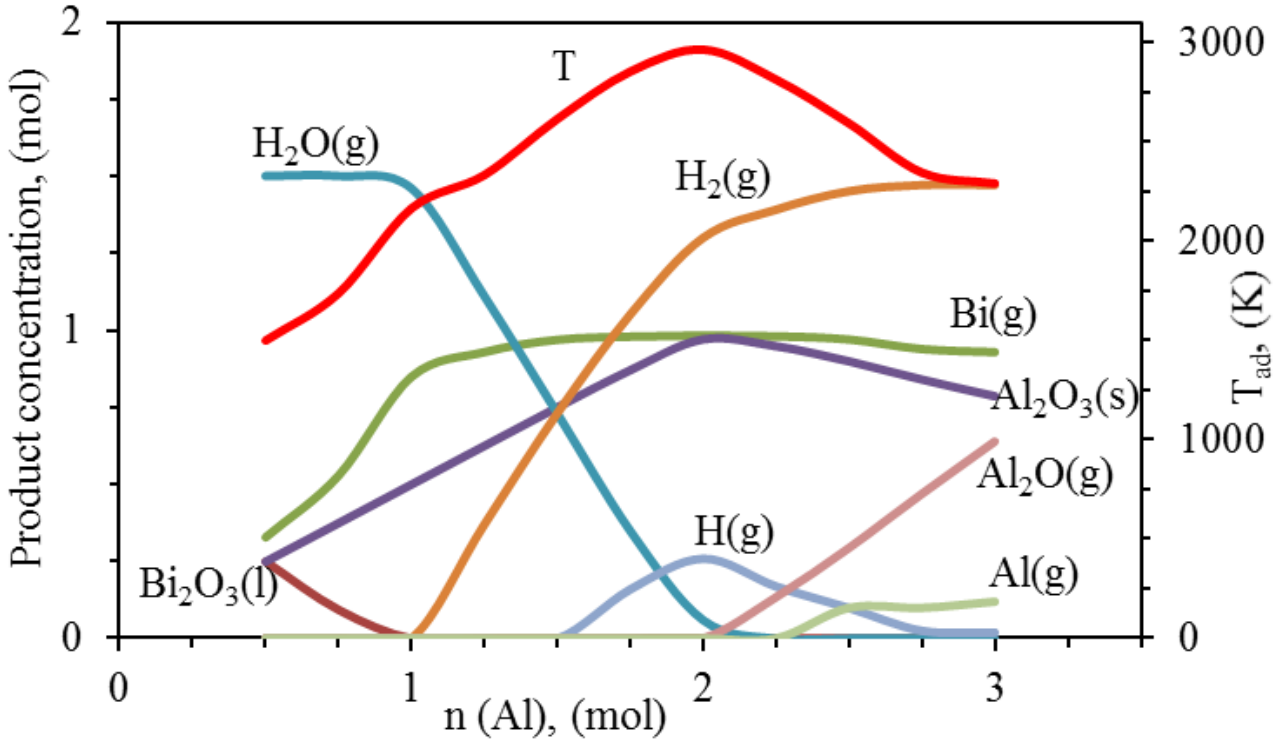

Figure 3-1. Dependence of the adiabatic temperature and equilibrium concentration of condensed and gaseous phases on fuel concentration during the exothermic reaction in system Al-$Bi(OH)_3$: (red line is adiabatic combustion temperature).

The system (3-2) appears to have higher energetic capacity per mass and per volume. However, if we assume that due to high temperatures about 3000 K only the Bi particles (boiling point at 1832 K (Cahill et al, 1963) and water will transform into gaseous phase (Al_2O_3 boiling point is 3250 K (Rowe et al, 2009), then gaseous products generated for system (3-2) per initial mixture mass is 0.00385 mol/g, while the system (3-1) generates twice higher amount of 0.0087 mol/g. This can be very important advantage of hydroxide systems over oxide type thermites for applications where high amount of gaseous products per initial charge mass is vital, such as micropropulsions and microthrusters for space applications (Martirosyan et al, 2012, Puchades et al, 2014, Rossi et al, 2007). When the molar ratio Al/$Bi(OH)_3$ increases from 0.5 to 1, the system

follows equation (1). However, when the ratio increases above 1, the temperature increases to more than 2000 K, resulting to gradual decomposition of water into hydrogen and the released oxygen is consumed for excess aluminum oxidation. At molar ratio 2 the highest adiabatic temperature was calculated to be 2970 K, where the products are about 1 mol solid Al_2O_3, 1 mol gaseous Bi, and ~1.6 moles of gaseous mixture of molecular H_2 and atomic hydrogen. At this point, the reaction pathway becomes

$$2Al + Bi(OH)_3 = Al_2O_3 + Bi(g) + 1.4H_2(g) + 0.2H(g) \qquad (3\text{-}3)$$

The further increase of fuel to oxidizer molar ratio results some partial decomposition of solid Al_2O_3 into Al_2O gaseous and Al gaseous, however the amount of atomic hydrogen is quickly decreasing due to reduction of adiabatic temperature. Thus, in our experiments we used molar ratio for Al and bismuth hydroxide to be 2 according to reaction (3-3). We also took into account the extra oxide shell mass on aluminum nanoparticles. In addition, we investigated the pressure discharge dependence on non-stoichiometric fuel to oxidizer ratio, for comparison with thermodynamic calculations.

3.3. Experimental Methods and Procedures

The aluminum nanoparticles with average particle size 100 nm (87 %, covered with 13 % Al_2O_3) used for nano-thermite preparation was purchased from Sigma Aldrich Co and stored under Nitrogen (99.98 %) to avoid any contamination and oxidation. Bismuth hydroxide (99 %) was purchased from Acros Organics. Bismuth trioxide Bi_2O_3 was purchased from Sigma Aldrich (99.9 %, 10 μm).

The $Bi(OH)_3$ particles were milled in High Energy Ball Mill (HSF-3, MTI Co) machine for up to 15 minutes. In the milling media, the ball to powder weight ratio was 10:1. The powder batch mass was 0.01 kg. We homogenized the $Bi(OH)_3$ in high-energy ball milling for up to 15

min with 5 min time increments, to control the effect of the mechanical activation on particle size reduction, decomposition energy of bismuth hydroxide, and oxidizing activity in the nanostructured system Al-$Bi(OH)_3$.

The milling energy applied during the mechanical activation decreases the particle size of bismuth hydroxide particles. We calculated the energy dose transferred to powder batch using the method described in Ref (Hobosyan and Martirosyan, 2017, Delogu and Deidda, 2004). The effect of milling time and treatment energy of Al-$Bi(OH)_3$ system on pressurization rate were determined.

The Al-$Bi(OH)_3$ nano-thermite formulations were prepared with various mass ratios, which are fuel rich to compensate the presence of aluminum oxide shell on metal nanoparticles. While stoichiometric mass ratio was 1.1:8.9, the ratio of 2:8 was found experimentally as the best ratio for highest pressure discharge value.

The thermite was mixed with roller ball mill in alumina jar with zirconia balls (5 mm in diameter) under hexane environment for 9 hours, and then dried under vacuum for 12 hours. The resulting nano-thermite powder was placed into cylindrical charge holder with 0.4 cm^3 volume (the bulk density was ~0.6 g/cm^3) for the charges of 0.2 g mass (for another set of experiments, the mass was increased up to 0.5 g to observe pressure discharge dependence on nano thermite mass). The holder was placed into Parr Instrument High Pressure Cylindrical Reactor with 0.342 L volume. The detonation was electrically triggered by Ni-Cr micro wire, the pressure signals were received by piezoelectric transducer with rated pressure/voltage values (Omega) and the signals were amplified and recorded trough Omega DAQ-3005 Data Acquisition board with signal acquisition frequency of 1 MHz.

The thermo-gravimetric analysis (TGA) was performed using Differential Scanning Calorimeter (DSC) with the sensitivity 0.1 μg (Q-600, TA Instruments). The measurements were made in Nitrogen atmosphere (99.98 % purity).

A Nicolet iS5 FTIR spectrometer (Thermo Scientific) with an ID-5 accessory was used to perform Fourier Transform Infrared (FTIR) spectroscopy on a small quantity (~5 mg) of powder that was pressed to receive a flat surface. The measurement was performed in the wavenumber range of 4000-400 cm^{-1}.

The XRD analysis was performed by Bruker D-2 Phaser with Cu K_α anode, in 2θ range 20-60, where the main peaks of bismuth hydroxide and oxide are distributed. The scans were taken with θ precision 0.02° and sample was rotated with 15 rpm to statistically increase the number of particles contributing to XRD signal intensity. To avoid statistical experimental parameters such as powder amount, surface flatness, number of particles in preferred directions etc, the peak intensities are given with relative intensity values, represented as a ratio between intensity of the peaks to the intensity of the highest peak for each sample.

The particle morphology, composition and size distribution analysis were performed with JEOL 7800F Field Emission Scanning Electron Microscope, equipped with Electron Dispersive X-ray Spectroscopy system (EX-37270VUP).

3.4. Results and discussion

3.4.1. Bismuth hydroxide particle characterization

The thermo-gravimetric analysis and differential scanning calorimetry of as-received and mechanically activated bismuth hydroxide powder is essential step to estimate the amount of absorbed humidity and observe the decomposition characteristics of oxidizer $Bi(OH)_3$. We

expect that upon heating bismuth hydroxide decomposes into bismuth oxide according to the following simplified reaction pathway:

$2Bi(OH)_3(s) \rightarrow Bi_2O_3\ (s) + 3H_2O\ (g)$ (mass reduction up to 10.4 wt. %) (3-4)

The decomposition of bismuth hydroxide is complicated and includes several steps. Figure 3-2a represents the heat flow and weight change dependence on temperature for $Bi(OH)_3$ as received powder. The blue line represents the weight change (wt. %), the green line shows the heat flow (W/g), and the red line indicates the points through which the heat flow peaks are integrated to estimate the energy required for decomposition (J/g). The DSC was pre-calibrated for heat flow curve integration. The decomposition of bismuth hydroxide starts at around 390 ºC with 28.8 J/g degradation energy. The second mass loss starts immediately at around 502 ºC with corresponding 78.5 J/g decomposition energy for the last step. The decomposition is essentially completed at around 590 ºC. The energy required for all steps of decomposition was around 107 J/g. After 600 °C no weight loss or thermal effect is recorded until 700 ºC, where occur only pure Bi_2O_3 phase. The overall mass loss is about 9.7 wt. %, close to theoretical estimation from Eq. 3-4. Thus, the as-received powder contains very small amount of Bi_2O_3 (the XRD measurements below confirm the presence of trace amounts of Bi_2O_3).

Milling bismuth hydroxide up to 10 min results in 3-step mass loss and significantly reduces the energy required for complete decomposition. Figure 3-2b represents DSC results for $Bi(OH)_3$ treated 10 min in high energy ball mill.

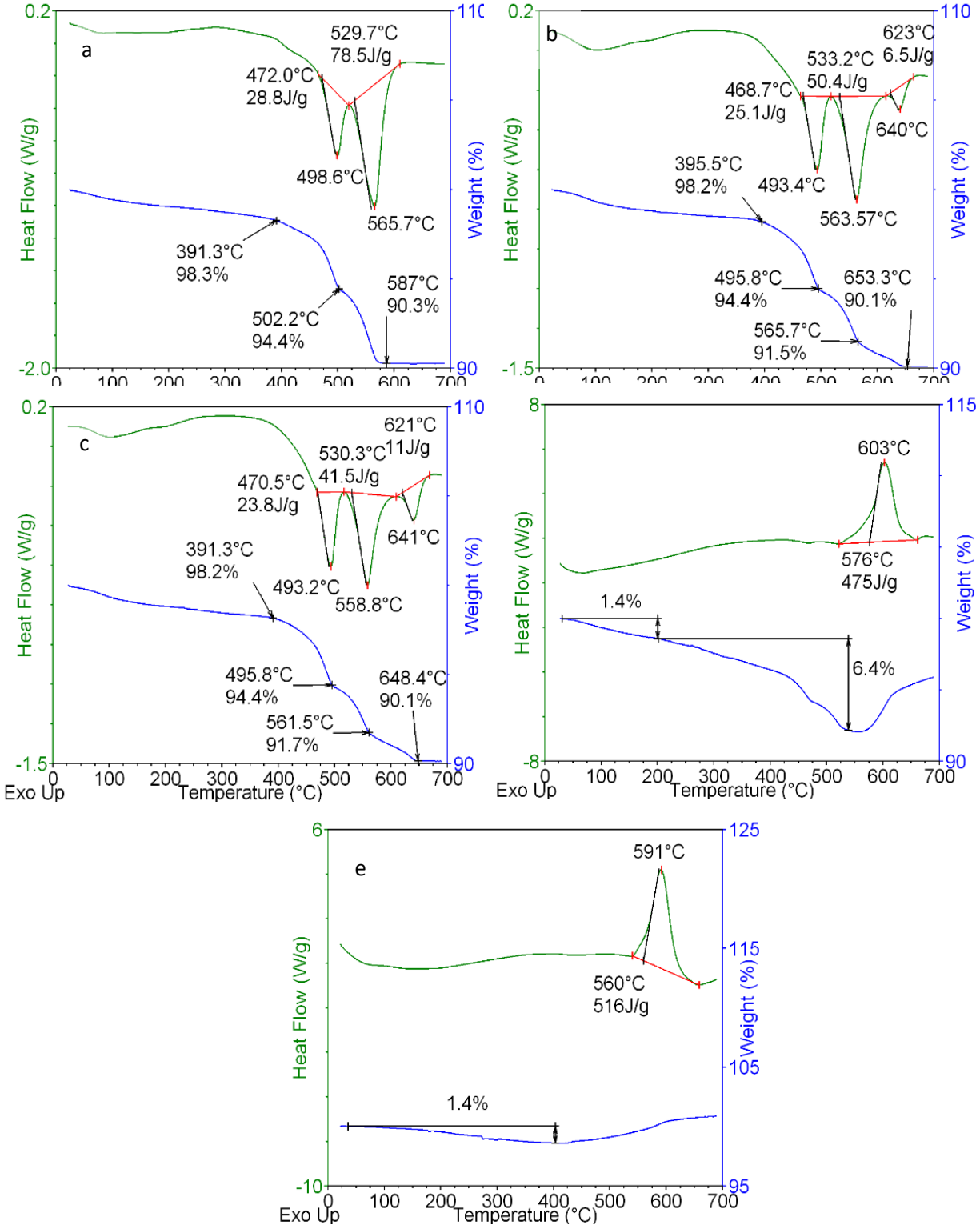

Figure 3-2. Heat flow and weight change dependence on the temperature for (a) as received $Bi(OH)_3$; (b) 10 min milled $Bi(OH)_3$; (c) 15 minutes milled $Bi(OH)_3$., d) Al-$Bi(OH)_3$ mixture, e) Al-Bi_2O_3 mixture

The weight loss starts at around 395 °C with 25.1 J/g energy consumption for the first step and demonstrated to the significant energy decrease for the second step from 78.5 J/g to 50.4 J/g with a new endotherm in the end by 6.5 J/g energy. This might be due to the increased defects in crystal structure, and the weight loss is also stretched and delayed in this case. Thus, the energy required for the complete decomposition is about 82 J/g, i.e. 23 % less than that for as-received $Bi(OH)_3$. Apparently, the milling not only reduces the particle size to sub-micrometer domain (see particle morphology characterization below), but also creates multiple defects in crystallographic structure, thus reducing the decomposition energy.

The further milling of particles does not bring significant changes in overall decomposition energy. For the particles milled for 15 min, the first step consumes 23.8 J/g energy, the second endotherm energy decreases to 41.5 J/g (Figure 3-2c) and the energy for last step increases to 11 J/g. The overall decomposition energy is about 76 J/g, 29 % less than that for as-received powder. The comparison of decomposition energies is especially important, because in nano-thermite some part of energy released from Al-$Bi(OH)_3$ will be consumed on oxidizer particle decomposition. Thus, lower decomposition energy of oxidizer is beneficial for the nano-thermite pressure discharge ability. Therefore, we expect that 15 min treated $Bi(OH)_3$ should give thermite with increase discharge energy. Further milling of bismuth hydroxide particles is not reducing the overall decomposition energy as presented in Figure 3, thus for further experiments were used $Bi(OH)_3$ particles milled up to 15 minutes.

To compare the heat release in the systems Al-$Bi(OH)_3$ and Al-Bi_2O_3, we performed DSC analysis of these systems (Figure 3-2d, e). Both mixtures were prepared in the same conditions (9 h mixing in hexane). The Al-$Bi(OH)_3$ system shows 475 J/g energy release at around 576 ºC (Fig. 3-2.d), which is about 8 % less than the exothermic peak in the Al-Bi_2O_3 system at around

560 ºC (516 J/g, Figure 3-2e). We should mention that before vigorous exothermic reaction the Al-$Bi(OH)_3$ composition has stepwise weight loss of about 7.8 wt. %, due to slow heating rate (20 ºC/min) some part of OH groups escape.

It is important to note, that Al-$Bi(OH)_3$ is practically stable up to 200 ºC, losing only about 1.4 wt. % due to evaporation of residual solvents and absorbed moisture. However, above 200 ºC we see gradual mass reduction up to ignition of nano-thermite at 550 ºC.

The dependence of decomposition energy of bismuth hydroxide particles on high energy ball milling time is presented in Figure 3-3. Longer times result in milling energy dose, but the decomposition energy is reduced at longer mechanical treatment times.

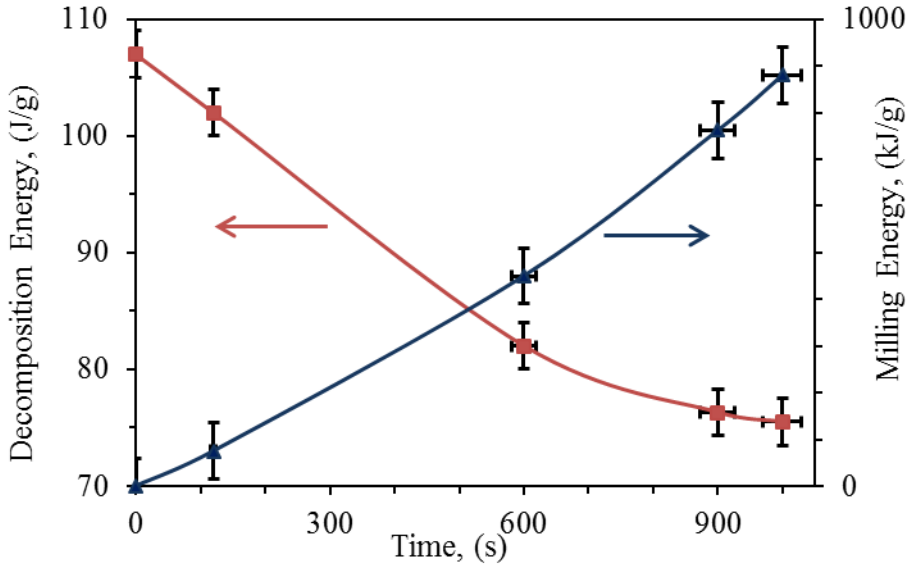

Figure 3-3. The decomposition energy and milling energy dependence on milling time for the $Bi(OH)_3$ particles.

The XRD measurements for as-received particles and the powder milled 15 min are presented in Figure 3-4a. The initial powder has sharper peaks, due to coarser particles size up to 100 μm (see SEM characterization below). The crystallite size was estimated to be 270 Å, using Sherrer`s formula (Martirosyan et al, 2009). The milling of the particles reduces the average

particle size to sub-micrometer and nano-size domain, and the crystallite size is reduced to 170 Å, and as a result appears broader peaks (15 min milled particles). The traces of bismuth oxide also disappear in the process of homogenization through the milling processes.

Figure 3-4b represents FTIR measurements for as-received particles of $Bi(OH)_3$ and 15 min milled $Bi(OH)_3$, as well as nano-energetic mixture Al-$Bi(OH)_3$. The absorption peaks at 600-800 cm^{-1} correspond to Bi-O-Bi bonds, while the peaks at 1100-1400 cm^{-1} correspond to Bi-OH groups (Bartonichkova et al, 2007). The reaction product did not have significant absorption in IR region.

The particle size and morphology observations with SEM show that as-received particles are coarse with up to 100 μm particle size demonstrated in Figure 3-5 a,b. Milling 10 minutes critically reduces the portion of micrometer-sized particles and produces mostly sub-micrometer, as well as nano-meter sized particles as shown in Figure 3-5 c,d. The increasing milling time up to 15 min results in higher amount of submicron and nano-meter sized particles (Figure 3-5 e,f) . Further increase of milling time after 15 minutes does not result in significant reduction in particle size.

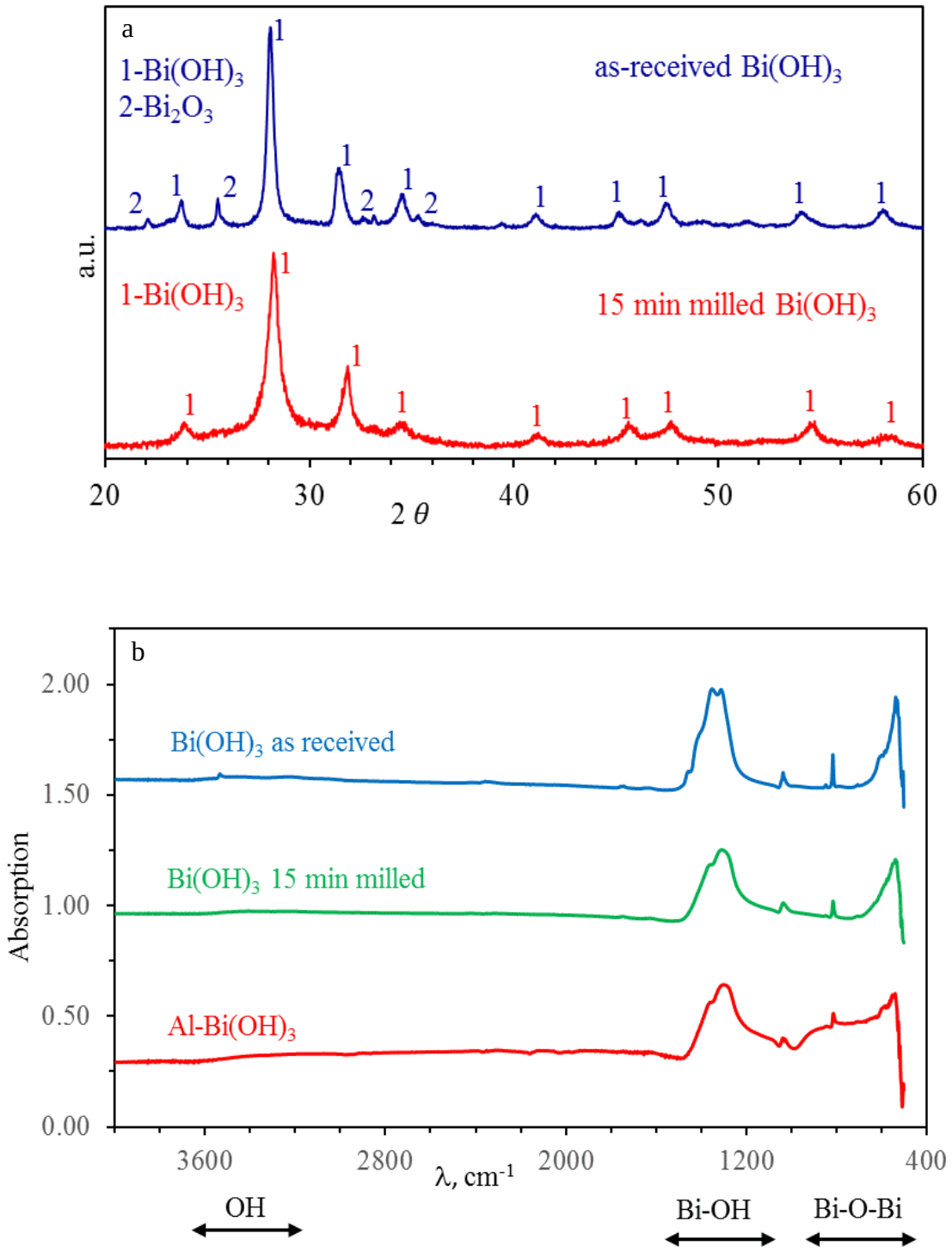

Figure 3-4. a) XRD patterns for as-received $Bi(OH)_3$ and 15 min milled $Bi(OH)_3$, b) FTIR absorption for as-received $Bi(OH)_3$, 15 min milled $Bi(OH)_3$, and Al-$Bi(OH)_3$ prepared using 15 min milled $Bi(OH)_3$

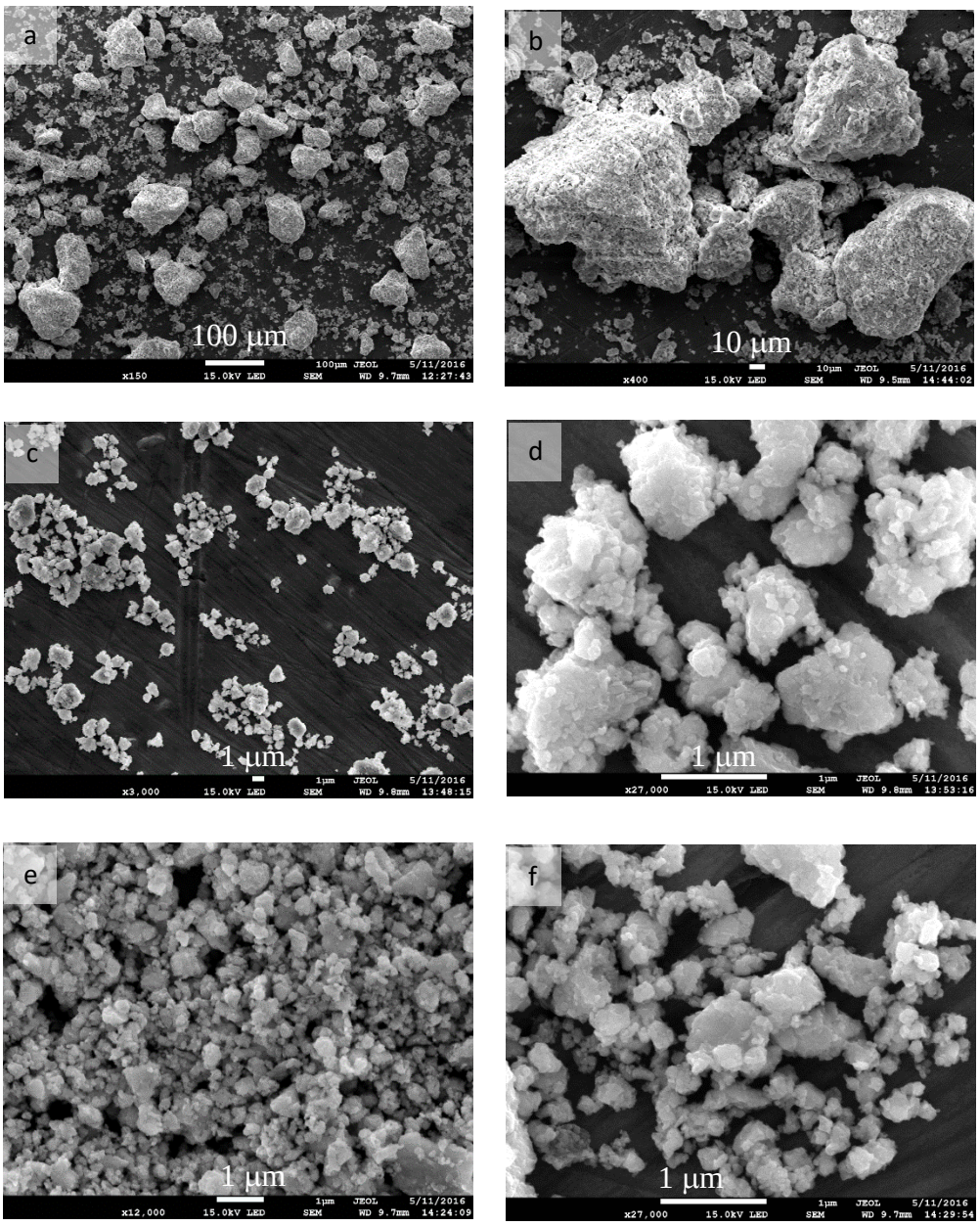

Figure 3-5. SEM images for (a, b) as received $Bi(OH)_3$; (c, d) 10 minutes milled $Bi(OH)_3$; (e, f) 15 minutes milled $Bi(OH)_3$.

The SEM image of nano-thermite Al with bismuth hydroxide (milled for 15 min) is presented in Figure 3-6a. The small (~100 nm) Al nanoparticles are well distributed in sub-micrometer sized $Bi(OH)_3$ media. The higher magnification image shows individual Al nanoparticles surrounding $Bi(OH)_3$ particles (Figure 3-6b). The EDS mapping of elemental Al and Bi for the same area shown in Figure 6a is presented in Figure 3-6c,d, respectively. The bar in the left side of maps is representing the relative concentration of element. The distribution of Al and Bi atoms is consistent with the corresponding particle locations.

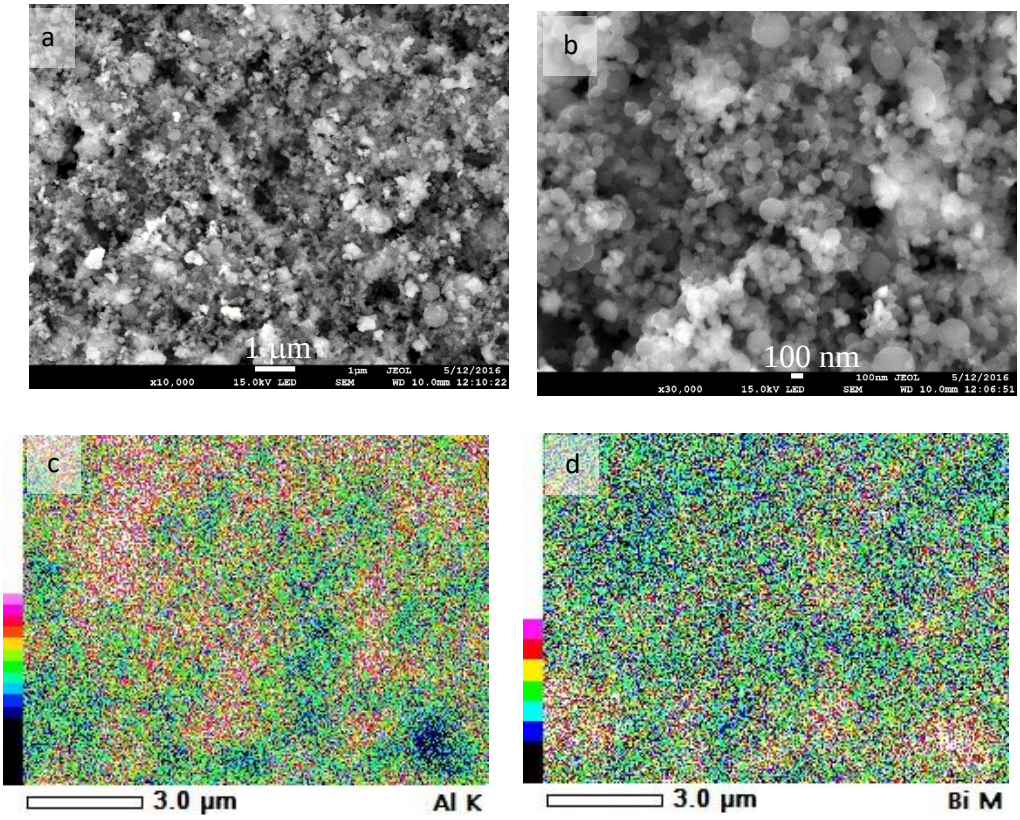

Figure 3-6. (a, b) SEM images of Al-$Bi(OH)_3$ (15 min milled) nano-thermite, bar length 1 µm and 100 nm, respectively; (c, d) EDX mapping for Al and Bi elements for the region shown in (a). The color bar represents the concentration of atoms

3.4.2. Pressure discharge in Al-$Bi(OH)_3$ system

The Al-$Bi(OH)_3$ thermite was prepared using Al nanopowder with average size 100 nm and bismuth hydroxide (as received, and milled for 10 and 15 minutes) at various fuel to oxidizer ratios. Figure 3-7 represents the pressure vs time plot for Al-$Bi(OH)_3$ thermites prepared with as received and treated $Bi(OH)_3$ powder up to 10 and 15 min with different weight percentages of Al. The highest pressure for thermite prepared with as-received $Bi(OH)_3$ was 3.33 MPa for 0.2g thermite, while value for 10 minute treated $Bi(OH)_3$ is 3.71 MPa (11 % pressure rise) and for 15 min treated $Bi(OH)_3$ is 4.34MPa (30 % pressure rise). For all cases the pressure fluctuates in near the peak value for about 20 microseconds. The nano-thermites prepared with bismuth hydroxide milled for longer time (up to 20 minutes) perform identical to 15-minute milled powder. The 20 wt. % Al and 80 wt. % $Bi(OH)_3$ thermite generates the highest pressure of 4.34 MPa compared to 2.67 MPa for 15 wt % Al and 2.41 MPa for 25 wt % Al containing thermites, for 0.2 g nano-thermite charge mass.

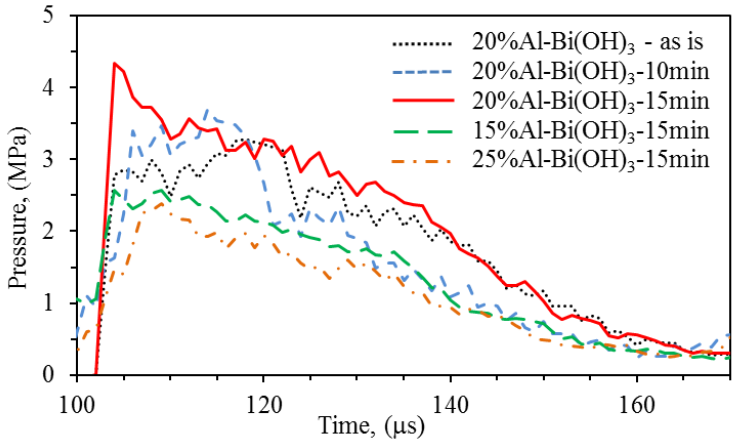

Figure 3-7. Discharge pressure dependence on time for Al-$Bi(OH)_3$ thermites prepared with as received, 10 and 15 min mechanical treated $Bi(OH)_3$, with 20 wt. %Al, and thermite prepared with 15 min treated $Bi(OH)_3$ and different weight percentages of Al.

Figure 3-8 represents the pressure discharge dependence on nano-thermite loading charge mass. This thermite was prepared with conventional roller mixing method, using 15 min treated $Bi(OH)_3$ and 20 wt % Al in hexane environment with mixing time up to 9 h. The specific multiplication factor for this thermite was ~14.44*m+0.6669 (i.e. 1 g loading charge would generate 15.1 MPa pressure in 0.342 L volume). The pressure*volume (PV) value for this powder per mass was 5.6 kPa*m^3/g, which is comparable to one of the highest values reported in nanoenergetic literature (Martirosyan, 2011).

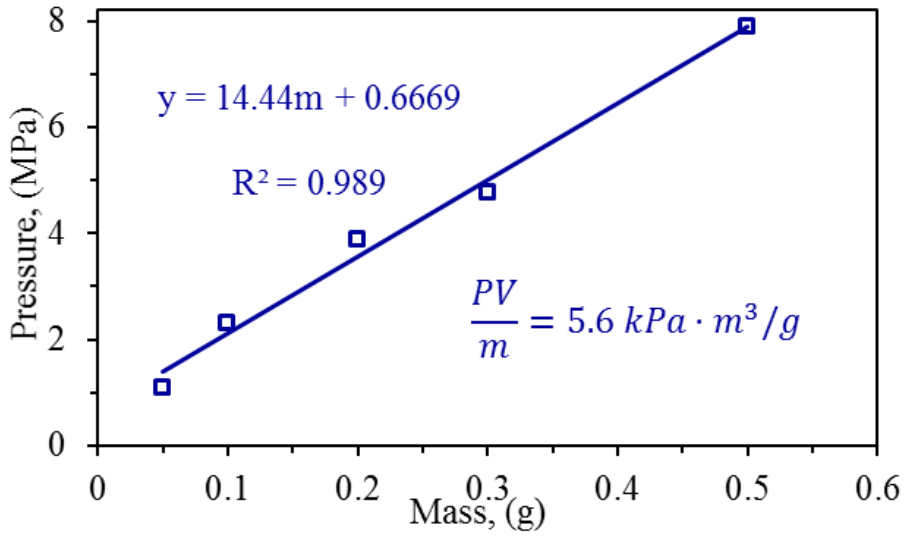

Figure 3-8. The pressure dependence on thermite weight for Al-$Bi(OH)_3$ nano-thermite.

CHAPTER IV

TAILORING BISMUTH HYDROXIDE AND OXIDE FLOWER-, BOWTIE- AND BRUSHWOOD-LIKE STRUCTURES THROUGH MICROFLUIDIC SYNTHESIS FOR NANOTHERMITES

4.1.Introduction

Bismuth oxide Bi_2O_3 is an important component of ferroelectric (Singh et al, 2009) and electrochemical supercapacitors (Yuan et al, 2009). Bi_2O_3 is used in the field of optical materials (Lu et al, 2015, Oprea et al, 2004), gas sensors, photocatalysts, solid oxide fuel cells, etc (Hanna, 2004, Azad et al, 1994). Being a strong oxidizer, Bi_2O_3 is also used in nanoenergetic materials called Nanoenergetic Gas-Generators (NGG), which are alternatives to traditional energetic materials including pyrotechnics, propellants, primers and solid fuels (Martirosyan, 2011). It was shown that bismuth oxide is one of the best oxidizers in the field of NGGs (Martirosyan, 2009, Wang et al, 2011). The synthesis of bismuth oxide particles with various shapes and size has focused significant attention. There were several attempts to synthesize flower-like bismuth oxide hierarchical structures (Tseng et al, 2010, Zhou et al, 2009, Chen et al, 2012, Xiao et al, 2015), but the formation mechanism was not well understood. Moreover, production of particles with various morphology, using an easily controllable method to tune the size and shape of bismuth oxide particles, is desired.

In this chapter, the effect of surfactant polyethylene glycol PEG with 200 and 8000 molecular weight, are evaluated for the preparation of bismuth oxide particles with various

morphology and size, using microfluidic synthesis approach. The microfluidic synthesis is preferred, because performing the synthesis with magnetic stirring produces broken structures (Li, 2006). During the violent mixing with magnetic stirrer, the formed particles tend to break into 1-10 μm irregular shaped segments. Thus, the microfluidic preparation is critical for preserving the complete structures of bismuth oxide particles. The flow dynamics along the microfluidic network is examined to quantitatively describe the complex structure formation for bismuth oxide particles. Furthermore, the impact of the particle shape on oxidizing activity of bismuth oxide in nanoenergetic formulation Al-Bi_2O_3 was studied.

4.2.Experimental Methods and Procedures

The $Bi(NO_3)_3*5H_2O$ (98 %) and NaOH (98 %) were purchased from Sigma Aldrich. HNO_3 concentrate (70 %, Sigma Aldrich) was diluted to receive 1.5 M concentration. Microfluidic pump (ISMATEC Reglo Digital, Peristaltic, MS-4/8) was used to synthesize bismuth oxide particles. The Y connector inner diameter was 0.5 mm connected to output channel with 0.76 mm diameter. As a bismuth source reagent, 0.7 g $Bi(NO_3)_3*5H_2O$ was added to 30 ml 1.5 M HNO_3, and sonicated for 30 minutes to completely dissolve the $Bi(NO_3)_3$, then 15 g PEG (200 or 8000, Sigma Aldrich) was added and sonicated for another 30 minutes. As a neutralizing reagent supplying hydroxide ions, a 4.5 g NaOH was dissolved in 45 ml H_2O by 1 h sonication.

Both reagents were placed near microfluidic pump, and were sent through separate tubes to Y-connector with 60 rpm pumping drive speed, and the product was collected from output microfluidic channel. The reaction between $Bi(NO_3)_3$ and NaOH took place in the presence of PEG macromolecules acting as a surfactant. The PEG-s with various molecular weight resulted in various shapes of end product Bi_2O_3. The product vial contained sodium nitrate, PEG, and

bismuth oxide particles. The end product pH value was between 13-13.5 in all cases. The $NaNO_3$ and PEG were removed from the end product by washing it with water and centrifuging 3 times. The product was dried under 65 ºC for 12 hours.

For the NGG preparation, the Al: Bi_2O_3 weight ratio was 2:8. For the preparation of 0.25 g mixture, 0.2 g Bi_2O_3 was added into 20 ml isopropanol (IROH, 99.5 %, Sigma Aldrich), and 0.05 g Al in 20 ml IROH, and both vials were sonicated in sonic bath for 30 minutes. 80 µl 0.1 % Poly-4-vinyl-pyridine (Sigma Aldrich) was added into Al-IROH solution for self-assembly, and both vials were sonicated for another 30 minutes. The water was changed in sonic bath to avoid heating of the liquids in vials. Al-IROH was added into Bi_2O_3-IROH solution and the mixture was sonicated for another 30 minutes. The suspension was transferred into glass container and placed in drier set to 65 ºC, and was dried 12 hours. The dry powder with 0.2 g charge mass was tested in modified Pharr reactor with 0.342 L volume, and equipped with pressure transducer and Omega data acquisition board with 1 MHz data acquisition speed. The voltage was converted into normalized pressure (MPa/g) and pressure discharge peaks were compared for bismuth oxide with various shapes.

4.3.Results and Discussion

The bismuth oxide particles prepared using PEG-200 surfactant were light yellow in color.

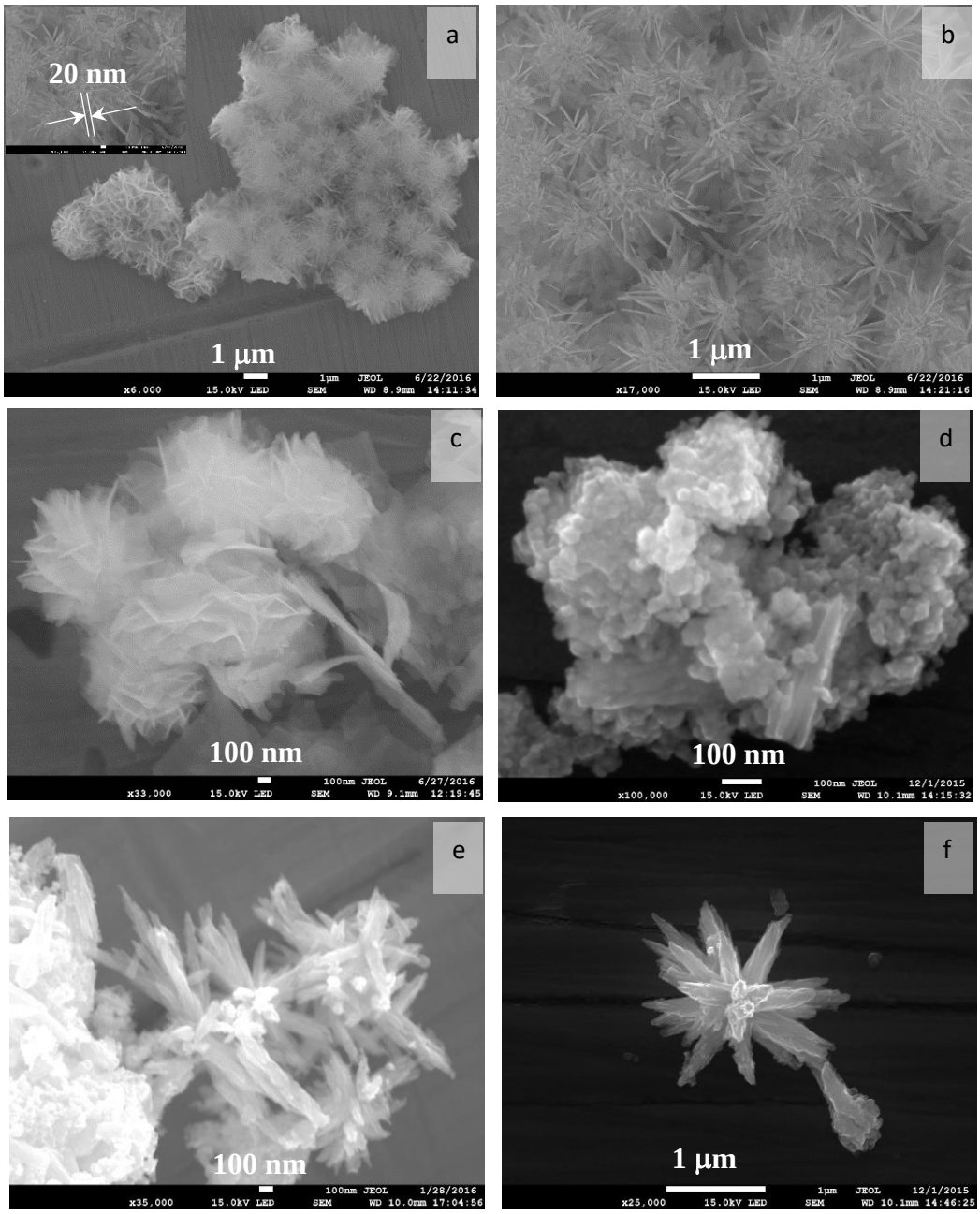

Figure 4-1. SEM images of Bi_2O_3 received in the presence of PEG-200 surfactant dried at room temperature (a, b, c) and 65^o C for 12 h (d, e, f).

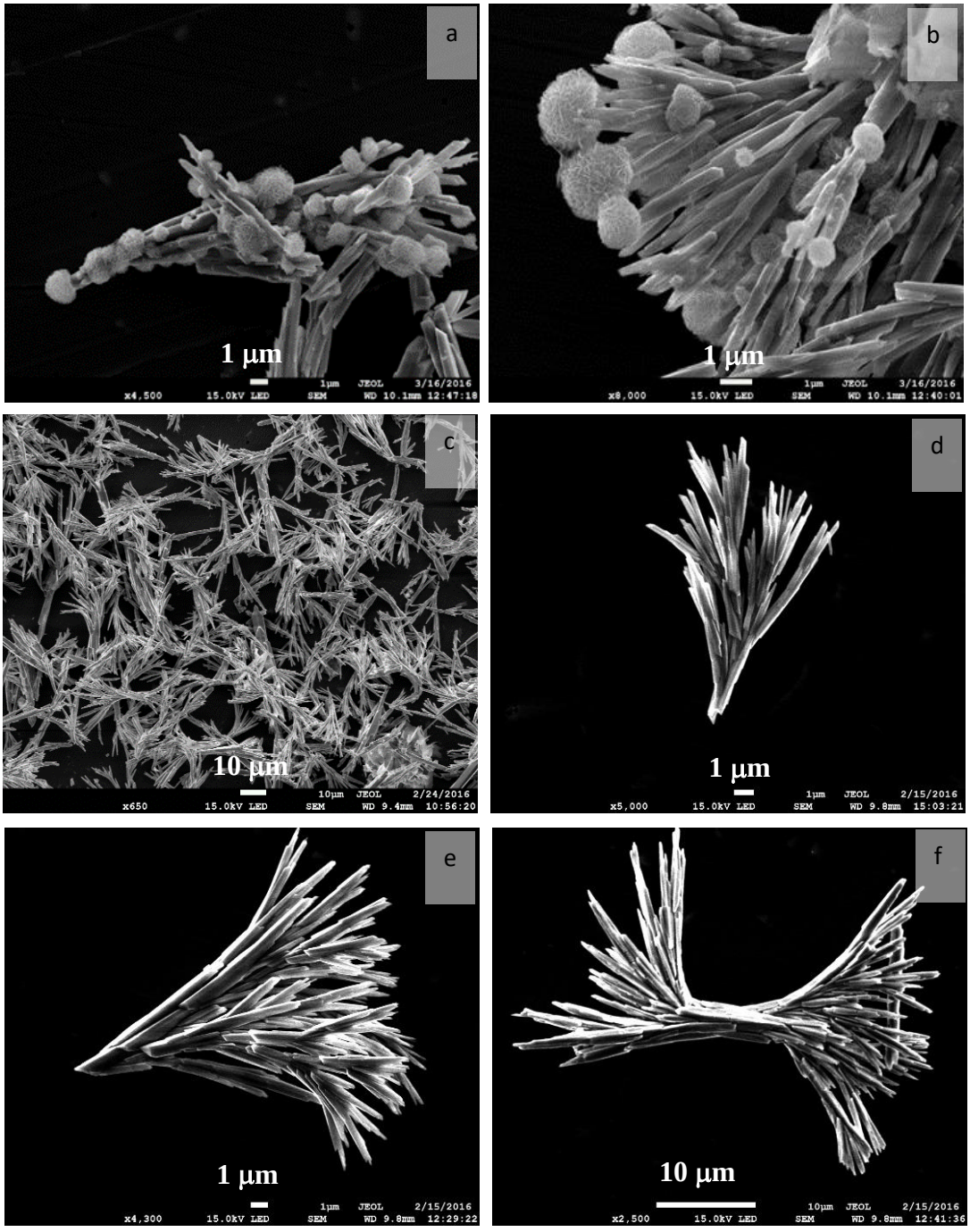

Figure 4-2. (a, b) SEM images of Bi_2O_3 received in the presence of PEG-8000 surfactant, showing flower-like structures, and (c) dried at 65 ºC showing (d, e) brushwood-like and (f) bowtie-like structures.

The drying condition of reaction products is an important parameter for particle morphology.

The SEM images displayed in Figure 4-1 (a-c) show that the particles dried at room temperature, are composed by layers of petals with thickness of 20-30 nm (Figure 4-1a inset), that are forming flower bud-shaped conformation with conglomerate diameter up to 2 μm. In the case of drying the particles at 65 ºC for 12 hours, some crystallization of nanoparticles takes place (Figure 4-1d, e), which can self-assemble into flower-like structures (Figure 4-1 f).

The particles prepared with PEG-8000 surfactant are presented in Figure 2. In some structures, spherical formations remain on the endpoints of rods, resembling flower bouquets (Figure 4-2. a, b).

However, drying these particles at 65 ºC for 12 hours removes all spheres. Presumably, the spherical formations merge into rods. The well-dried particles have brushwood-like and bowtie-like structures (Figure 4-2 c-f). We note that the rods are growing from common stalk, where the individual rods are further branched, much like in a brushwood (Figure 4-2 d, e). Many of these structures are connected through common stalk from opposite directions, forming bowtie-like conformations (Figure 4-2 f). It is possible, that the separate brushwood-like structures were connected to each other like bowties, but during movement through microfluidic channel, or during product washing they broke from stalk, leaving two brushwood-like structures. The absence of individual rods broken from brushwood-like structures is the result of highly lamellar, calm flow of the product through Y-connector and tubes of microfluidic pump.

The XRD analysis of product powder received with PEG-200 surfactant showed that the particles were amorphous, and exhibited small peaks of Bi_2O_3 and $Bi(OH)_3$, as can be seen in

Figure 4-3a, (red line). The peak of Bi_2O_3 is α phase, which is the room temperature phase of Bi_2O_3. The particles received by addition of PEG 8000 instead of PEG-200 are highly crystalline, as can be seen from Figure 4-3 a, (blue line). The multiple peaks are corresponding to α phase Bi_2O_3, with only one small peak representing bismuth hydroxide.

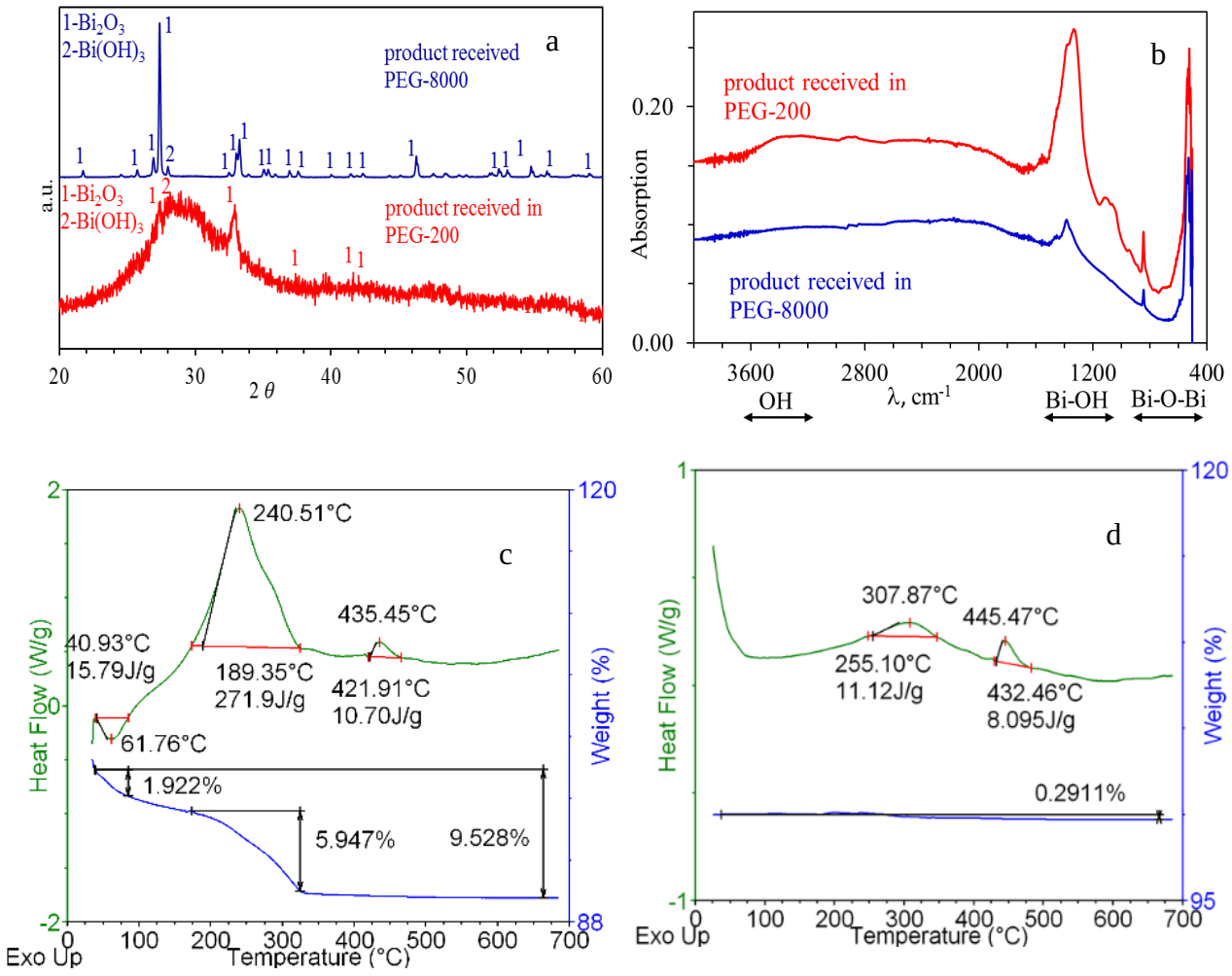

Figure 4-3. (a) XRD analysis for product received using PEG 200 and PEG 8000, (b) FTIR analysis for product received using PEG 200 and PEG 8000, (c) DSC-TGA analysis for product received using PEG 200, (d) DSC-TGA analysis for product received using PEG 8000.

We performed FTIR absorption spectroscopy, which gives the opportunity to differentiate between OH groups connected to Bi atoms in the 1100-1600 cm^{-1} regions [55], as opposed to OH groups present as moisture in 3200-3600 cm^{-1} wavenumbers (Figure 4-3 b).

The product received in the presence of PEG-200 shows a strong absorption of OH groups connected to Bi, while the product received with PEG-8000 shows only slight absorption intensity for the Bi-OH bond. Both products were dried at the same temperature (65 ºC) for the same period of time (12 hours). Thus, the low temperature drying is not responsible for strong Bi-OH absorption in powder received with PEG-200.

In order to quantitatively evaluate the amount of OH groups, as well as the remnant PEG and moisture in the product, we performed thermogravimetric analysis (TGA) in addition to differential scanning calorimetry (DSC). The DSC/TGA analysis of bismuth oxide received with surfactant PEG-200 is presented in Figure 4-3 c. The residual moisture of about 2 wt. % is evaporated before 100 ºC with 15.8 J/g evaporation energy. Above 200 ºC it was observed 6 wt. % weight loss with 272 J/g exothermic effect indicating that some residual amounts of PEG remains in the product and decays in the air. The decomposition of bismuth hydroxide should be expected at temperatures above 400 ºC, as discussed in Chapter 3. Thus, we may have partially hydroxylated bismuth oxide, $Bi_x(OH)_yO_z$, which is decomposing during PEG-200 combustion, and OH groups are leaving the system before 350 ºC. The overall weight loss up to 700 ºC is 9.5 wt. %, which indicates that these particles are above 90 wt. % Bi_2O_3. At 435 ºC, an exothermic effect is observed without weight loss, which corresponds to phase transition between α–phase (at room temperature) to β–phase (at higher temperature) of Bi_2O_3. For the product received using PEG-8000 surfactant, the DSC-TGA shows above 99 wt. % Bi_2O_3 (Figure 4-3 d). About 0.3 wt. % weight reduction was observed with small amount of PEG burning at 255 ºC and α–β

phase transformation at 445 ºC with 8 J/g energy. Thus, the particles received with PEG-8000 are ~ 99 wt. % bismuth trioxide with highly crystalline structure.

In order to understand the particle structure formation dynamics in microfluidic channels, we examined the flow characteristics and the residence time of particles during movement through the microtubes.

The viscosity of product solution was estimated using falling sphere method with wall (W) and ends (E) correction (Webster et al, 2014), according to

$$\eta = 2gr_s^2 \frac{(\rho_s - \rho_l)W}{9V_t E} \qquad (4\text{-}1)$$

where r_s is the radius and ρ_s is the density of falling sphere through the liquid which has ρ_l density, V_t is the sphere falling terminal velocity, *W* and *E* are the correction factors for the sphere falling through cylindrical container of radius r_c and height H, and are calculated by

$$W = 1 - 2.104\left(\frac{r_s}{r_c}\right) + 2.09\left(\frac{r_s}{r_c}\right)^3 - \left(\frac{r_s}{r_c}\right)^5 \qquad (4\text{-}2)$$

$$E = 1 + 3.3\left(\frac{r_s}{H}\right) \qquad (4\text{-}3)$$

The wall correction is for $0.16 \leq {}^{r_s}/_{r_c} \leq 0.32$. The viscosity of the reaction product was estimated $\eta = 0.052\ Pa * s$, which is 52 times higher than that for water. We estimated the highest speed *V* of particles moving through microfluidic tube 30 mm/sec, and the Reynold`s number was calculated according to $Re = \rho_l VD/\eta$, where D is the channel diameter 0.76 mm. The Reynolds number for the flow was 0.48, which indicates highly laminar flow of liquid through channels, as it is much less than the accepted 2100-2300 turbulence value for flows in micro-channels (Bird et al, 1960). The schematics of microfluidic network is illustrated in Figure 4-4 a. The tubing is

divided into 3 reaction zones extending to 1 cm, 20 cm and 40 cm distances. The bismuth oxide is formed in the Y connector chamber and is moving through the reaction zone 1, which has 0.5mm tubing diameter. The reaction zone 2 starts at 1 cm and ends at 20 cm, and has tubing diameter 0.76 mm.

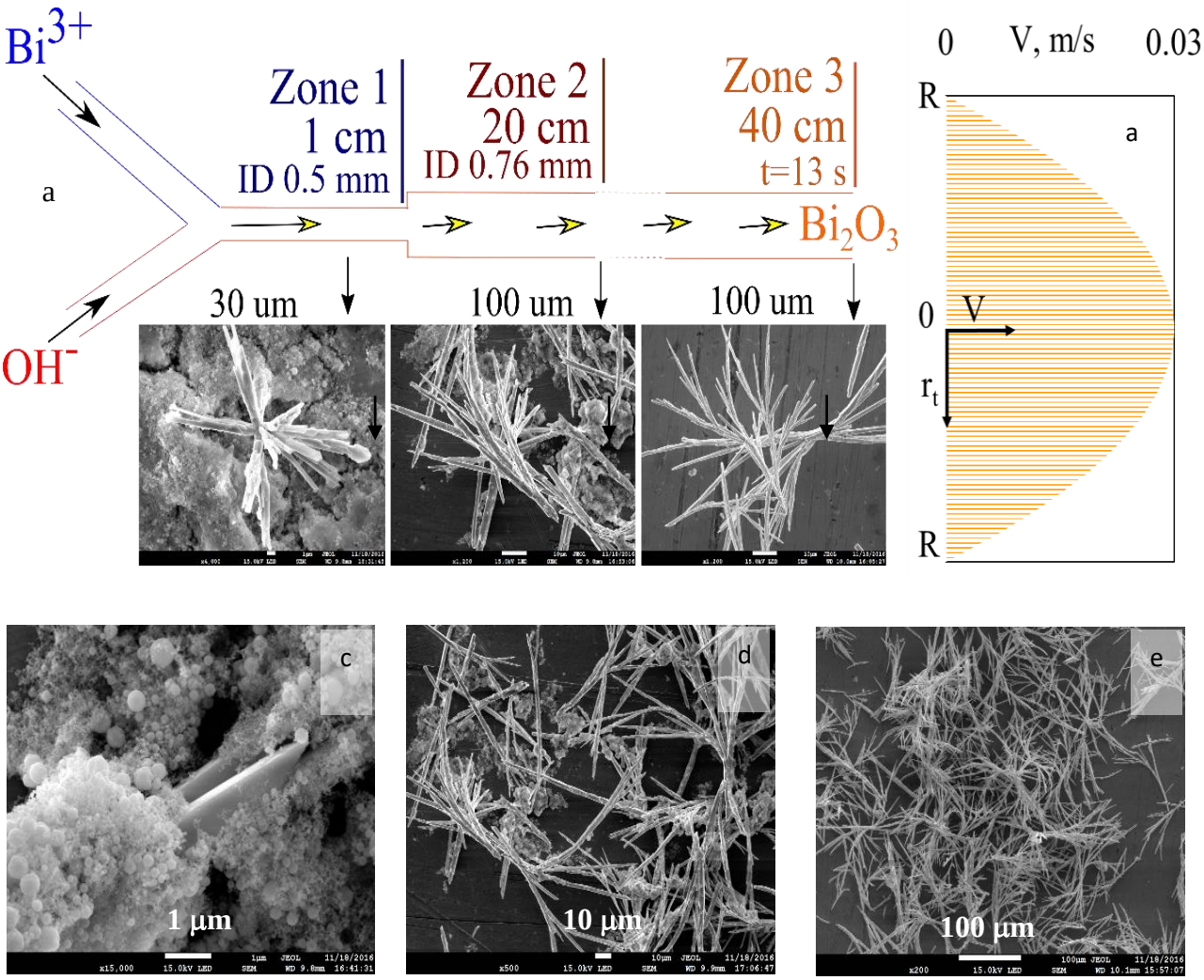

Figure 4-4. (a) The schematics of Bi_2O_3 formation in microfluidic network, (b) the velocity distribution in microfluidic channel with radius R=0.38 mm, (c, d, e) The morphology of particles extracted at 1, 20 and 40 cm distances from reaction chamber, respectively.

The zone 3 starts at 20 cm and ends at 40 cm, and has tubing diameter 0.76 mm. We collected the particles at the end of each zone at distances 1, 20 and 40 cm from the Y-connector center, as indicated in Figure 4-4a insets.

The following analysis is for the flow during various zones. For the lamellar flow, the parallel layers of liquid are moving at various speed at the center and near the tube walls. We calculated the velocity distribution of flow according to

$$V_z = \frac{(P-P_0)R^2}{4\eta L}\left[1-\left(\frac{r_t}{R}\right)^2\right] \qquad (4\text{-}4)$$

where $V = \frac{(P-P_0)R^2}{4\eta L}$ is the velocity at the center of the tube, (P-P_0) is the pressure difference that the microfluidic pump can create, L is the tube length, R is the tube radius (0.38 cm), and r_t is the distance from center (Bird et al, 1960).

The velocity distribution is parabolic (Figure 4-4 b), where the particles in the center of the tube have the highest velocity 30 mm/s and the residence time of particles in tube is about 6.7 s since length of this zone was 20 cm. The particles at 0.5R are moving slower, and the residence time for the same length 20 cm is about 33 % longer, while the particles at 0.9 R from the center exhibited four times longer residence time. The particles which have longer residence time in tubes, have more complete structure due to full interaction between reagents. The particles moving near the center have higher moving speed up to 3 cm/s, and shorter residence time, and do not fully develop to complete structures. We collected the particles at the end of each reaction zones, at tubing distance 1, 20 and 40 cm from the Y-connector center, as indicated in Figure 4-4a insets and Figure 4-4 c-e. The particles collected at 1 cm have the shortest residence time of about 0.5 s, after which the reaction was interrupted by rapid dilution in water. The SEM images

(Figure 4-4a inset and 4-4c) show 50-200 nm spherical seeds, although some rods are already starting to grow from common stalk. The particles collected at 20 cm distance with residence time at least 6.7 s have more complete structures. However, there is still significant amount of spherical particles which were presumably moving with high speed (~3 cm/s) through the center of tube, which had the shortest residence time, and did not manage to grow yet (Figure 4-4d). However, the particles collected at 40 cm with at least 13 s residence time are fully grown into complete structures with no evidence of spherical seeds (Figure 4-4e).

The SEM images of nano-energetic mixtures prepared with Bi_2O_3 received using surfactant PEG with various lengths is presented in Figure 4-5 insets. The bismuth oxide structures (prepared with PEG-200) are broken into smaller particles, which are self-assembling with aluminum nanoparticles (Figure 4-5 inset, left). The brushwood-like bismuth oxide structures received in the presence of PEG-8000 surfactant mostly are preserved, with Al nano-particles assembled in between branched rods (Figure 5 insets, right).

The pressure discharge peaks of these mixtures (Figure 4-5) show that the highest pressure was observed when was used Bi_2O_3 prepared in PEG-200 media, with 14.3 MPa/g normalized pressure value. The pressure x volume (PV) value for this powder per mass was 4.9 kPa m^3 g^{-1}, which is comparable to the 5.6 kPa m^3 g^{-1} value for Al-$Bi(OH)_3$ mixture (Hobosyan et al, 2016). The particles prepared with bismuth trioxide synthesized by using PEG-8000 produce 9 MPa/g (3.1 kPa m^3 g^{-1}) normalized pressure.

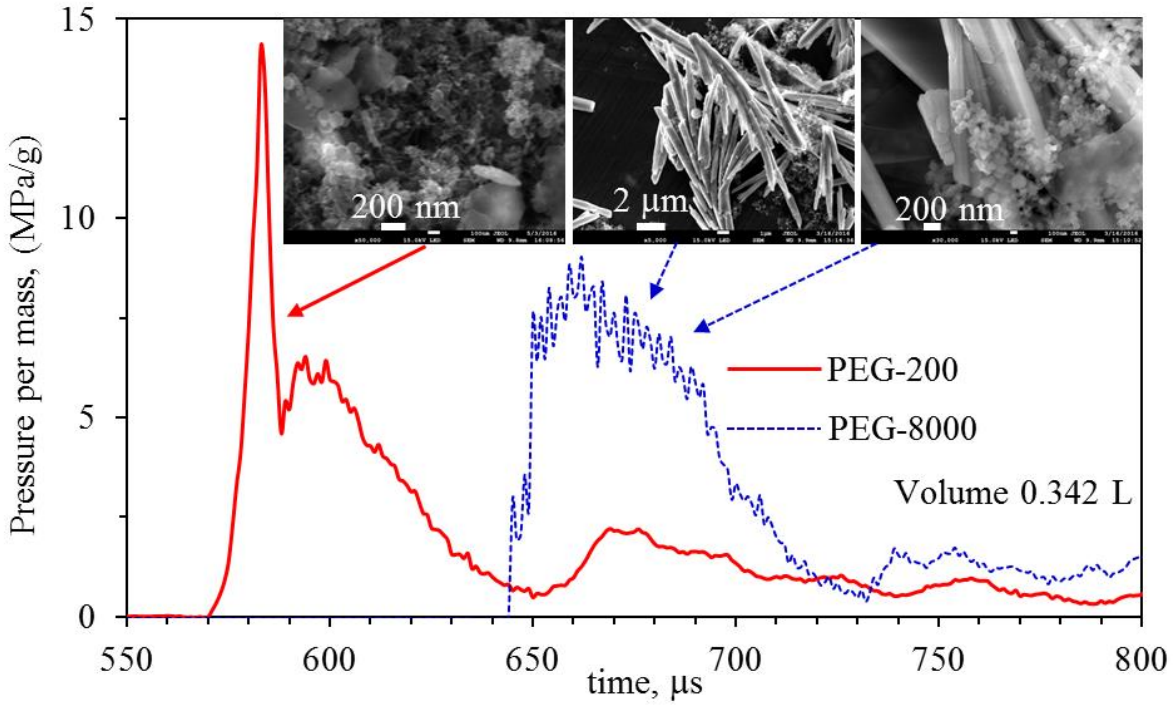

Figure 4-5. Pressure-time graphs for NGGs prepared with Al and Bi_2O_3 synthesized using PEG-200, and PEG 8000 surfactants, insets - SEM images of corresponding powder mixtures.

Thus, the flower-like particles, which are smaller and have higher amount of OH groups, produce ~60 % higher pressure than the brushwood-like structures, which are composed of primarily bismuth oxide with no OH groups in the structure. The reason of higher pressure in mixture containing bismuth oxide received using PEG-200 surfactant, might be the smaller oxidizer size, and the presence of compound with higher gas generation ability (OH groups in $Bi(OH)_3$, as discussed in chapter 3).

CHAPTER V

CONCLUSIONS

Nano-thermites gas generators are an emerging field of energetic materials with numerous applications. Oxides have been studied extensively for these systems. On the other hand, hydroxides have been neglected despite proving to be just as energetic and often better gas generators. A recent study (Hobosyan et al, 2016) has shown that the Al-$Bi(OH)_3$ system is highly exothermic and can be used as a strong gas generator. In this paper, theoretical predictions have been made for 22 exothermic nano-thermites, most of which demonstrate up to 3000 K adiabatic combustion temperature and could generate over 2 L/g gaseous products. Successful fabrication of these systems may prove to be challenging, yet if they are correctly manufactured they will conceivably behave as predicted by thermodynamics. According to the thermodynamic calculations, four systems based on bismuth, copper, cerium, and nickel hydroxides were prepared and tested for energy release and pressure discharge values, which demonstrate the reliability of calculations. All four mixtures were stable below 150 ºC, and have ignition temperature between 570-600 ºC with highly exothermic interaction behavior between aluminum and corresponding hydroxides. The highest pressure discharge was observed for Al-$Bi(OH)_3$ formulation, demonstrating pressure discharge about 3.3 MPa for 0.2 g mixture, one of the highest reported in literature.

Al-$Bi(OH)_3$ is a novel and powerful nano-energetic system with pressure discharge values comparable to one of the most powerful systems Al-Bi_2O_3. According to the thermodynamic calculations, this mixture generated twice higher gas generation abilities near the stoichiometric molar ratio at 2:1 for fuel to oxidizer ratio, compared to Al-Bi_2O_3 system, which is important for applications using high amounts of gaseous products such as microthrusters. The homogenization of bismuth hydroxide micro-sized particles in high energy ball mill for 15 minutes converts the particles to sub-micrometer and nano-sized domain, and reduces the decomposition energy by about 30 %. The resulting bismuth hydroxide powder is highly reactive and mixing with aluminum forms nano-thermite generating discharge energy up to 5.6 $kPa \cdot m^3/g$. The best mass ratio for generating highest pressure discharge value was 2:8 fuel to oxidizer. Metal hydroxides are promising components for nano-thermites that may generate vigorous amount of gaseous products and have extreme pressure discharge abilities.

Microfluidic synthesis is a convenient and flexible method to produce bismuth oxide particles with sizes between 1 to 60 μm. The PEG-200 surfactant allows to produce flower-like bismuth oxide conglomerates with up to 2 μm size. The utilization of PEG-8000 surfactant results in brushwood-like and bowtie-like structures with up to 60 μm size. For the particles received in the presence of PEG-8000 surfactant, the fluid dynamics calculations showed that the flow in micro-channels is highly laminar with Reynolds number 0.48. The velocity distribution in micro-channel is parabolic with highest value 30 mm/s. The complex structures are completed at the end of micro-channel tubes, if the residence time is at least 13 s. The XRD results show that product particles are mostly α-phase Bi_2O_3 at room temperature. However, the flower-like particles received in PEG-200 are amorphous with wide XRD peak corresponding to Bi_2O_3 and $Bi(OH)_3$, while the brushwood-like micro-sized particles are highly crystalline and contain α-

Bi_2O_3 phase. The FTIR confirms higher amount of OH groups in the product received with PEG-200 surfactant. The DSC/TGA analysis shows that flower-like particles contain up to 9.5 wt. % residual moisture and PEG burns at around 200 ºC with about 200 J/g energy release, while the brushwood-like and bowtie-like particles contain less than 1 wt. % moisture and PEG which burns at around 250 ºC. All particles show α−β phase transition at around 450 ºC with about 9 J/g energy release. The NGG prepared with flower-like and brushwood-like bismuth oxide particles shows that both mixtures are powerful nano-energetic materials. The formulation containing brushwood-like particles yields 3.1 kPa m^3 g^{-1} pressure discharge value, while the mixture prepared with flower-like particles produced ~60 % higher pressure discharge value of 4.9 kPa m^3 g^{-1}, which is comparable well to some of the most powerful formulations reported in literature (Martirosyan 2011, Hobosyan et al, 2016).

REFERENCES

Arnáiz, Francisco J., Rafael Aguado, and Susana Arnáiz. "Microscale thermite reactions." J. Chem. Educ 75, no. 12 (1998): 1630.

Azad, A. M., S. Larose, and S. A. Akbar. "Bismuth oxide-based solid electrolytes for fuel cells." Journal of materials science 29, no. 16 (1994): 4135-4151.

Baijot,V, L. Glavier, J.-M. Duc´er´e, M. Djafari Rouhani, C. Rossi and A. Est`eve, Modeling the Pressure Generation in Aluminum-Based Thermites, Propellants, Explos., Pyrotech., 2015, 40(3), 402–412.

Bartonickova, Eva, Jaroslav Cihlar, and Klara Castkova. "Microwave-assisted synthesis of bismuth oxide." Processing and Application of Ceramics 1, no. 1 (2007): 29-33

Bird, R. Byron, Warren E. Stewart, and Edwin N. Lightfoot. "Transport Phenomena John Wiley & Sons."

Bouma, Richard HB, Denise Meuken, Ries Verbeek, Maria Martinez Pacheco, and Laurens Katgerman. "Shear Initiation of Al/MoO3-Based Reactive Materials." Propellants, Explosives, Pyrotechnics 32, no. 6 (2007): 447-453.

Cahill, J. A., and A. D. Kirshenbaum. "The density of liquid bismuth from its melting point to its normal boiling point and an estimate of its critical constants." Journal of Inorganic and Nuclear Chemistry 25, no. 5 (1963): 501-506

Carney, C. S., R. E. Chinn, Ö. N. Doğan, and M. C. Gao. "Isothermal decomposition kinetics of nickel (II) hydroxide powder." Journal of Alloys and Compounds 644 (2015): 968-974.

Chen, Lang, Rui Huang, Shuang-Feng Yin, Sheng-Lian Luo, and Chak-Tong Au. "Flower-lBi2O2 CO3: facile synthesis and their photocatalytic application in treatment of dye-containing wastewater." Chemical engineering journal 193 (2012): 123-130.

Cheng, J. L., H. H. Hng, H. Y. Ng, P. C. Soon, and Y. W. Lee. "Synthesis and characterization of self-assembled nanoenergetic Al–Fe 2 O 3 thermite system." *Journal of physics and Chemistry of Solids* 71, no. 2 (2010): 90-94.

Cheng,J, L., H. H. Hng, H. Y. Ng, P. C. Soon and Y. W. Lee, Synthesis and characterization of

self-assembled nanoenergetic Al Fe2O3 thermite system, J. Phys. Chem. Solids, 2010, 71(2), 90–94.

Clark, Billy R., and Michelle L. Pantoya. "The aluminium and iodine pentoxide reaction for the destruction of spore forming bacteria." *Physical Chemistry Chemical Physics* 12, no. 39 (2010): 12653-12657.

Comet, Marc, Vincent Pichot, Benny Siegert, Fabien Schnell, Fabrice Ciszek, and Denis Spitzer. "Phosphorus-based nanothermites: a new generation of energetic materials." Journal of Physics and Chemistry of Solids 71, no. 2 (2010): 64-68.

Delogu, F, C. Deidda, "A quantitative approach to mechanochemical processes", J. Mater. Science, 39, pp.5121–5124, 2004

Demitrios, S, Z. Jiang, V. K. Hoffmann, M. Schoenitz and E. L. Dreizin, Fully dense, aluminum-rich Al–CuO nanocomposite powders for energetic formulations, Combust. Sci. Technol., 2008, 181(1), 97–116.

Dlott, D. D. "Thinking big (and small) about energetic materials." Materials science and technology 22, no. 4 (2006): 463-473.

Dreizin, Edward L. "Metal-based reactive nanomaterials." Progress in Energy and Combustion Science 35, no. 2 (2009): 141-167.

Granier, John J., and Michelle L. Pantoya. "Laser ignition of nanocomposite thermites." Combustion and Flame 138, no. 4 (2004): 373-383.

Greiner W., Neise L., Stöcker H. (1995). "Thermodynamics and statistical mechanics." Springer-Verlag. 101.

Hanna, Tracy A. "The role of bismuth in the SOHIO process." Coordination chemistry reviews 248, no. 5 (2004): 429-440.

Hobosyan, M., A. Kazansky, and K. S. Martirosyan. "Nanoenergetic composite based on I2O5/Al for biological agent defeat." In Technical Proceeding of the 2012 NSTI Nanotechnology Conference and Expo, pp. 599-602. 2012.

Hobosyan, Mkhitar A., and Karen S. Martirosyan. "Iodine Pentoxide Nano rods for High Density Energetic Materials." Propellants, Explosives, Pyrotechnics (2017).

Kevin, M, M. L. Pantoya and S. F. Son, Combustion behaviors resulting from bimodal aluminum

size distributions in thermites, J. Propul. Power, 2007, 23(1), 181–185.

Li, Wei. "Facile synthesis of monodisperse Bi2O3 nanoparticles." Materials chemistry and physics 99, no. 1 (2006): 174-180.

Lu, Yan, Yan Zhao, Jingzhe Zhao, Yuehong Song, Zhifang Huang, Fangfang Gao, Na Li, and Yawen Li. "Induced Aqueous Synthesis of Metastable β-Bi2O3 Microcrystals for Visible-Light Photocatalyst Study." Crystal Growth & Design 15, no. 3 (2015): 1031-1042

Martirosyan, Karen S., Mkhitar Hobosyan, and Sergey E. Lyshevski. "Enabling nanoenergetic materials with integrated microelectronics and MEMS platforms." In Nanotechnology (IEEE-NANO), 2012 12th IEEE Conference on, pp. 1-5. IEEE, 2012.

Martirosyan, K. S., L. Wang, A. Vicent, and D. Luss. "Synthesis and performance of bismuth trioxide nanoparticles for high energy gas generator use." Nanotechnology 20, no. 40 (2009): 405609.

Martirosyan, Karen S., Leizheng Wang, Arol Vicent, and Dan Luss. "Nanoenergetic Gas Generators: Design and Performance." Propellants, Explosives, Pyrotechnics 34, no. 6 (2009): 532-538.

Martirosyan, Karen S., L. Wang, and D. Luss. "Novel nanoenergetic system based on iodine pentoxide." Chemical Physics Letters 483, no. 1 (2009): 107-110.

Martirosyan, K. S., L. Wang, A. Vicent, and D. Luss. "Synthesis and performance of bismuth trioxide nanoparticles for high energy gas generator use." Nanotechnology 20, no. 40 (2009): 405609.

Martirosyan K. S., “Nanoenergetic gas generators, principle and applications,” J. Materials Chemistry, vol. 21, pp. 9400-9405, 2011.

Kim, Soo H., and Michael R. Zachariah. "Enhancing the rate of energy release from nanoenergetic materials by electrostatically enhanced assembly." Advanced Materials 16, no. 20 (2004): 1821-1825.

Martirosyan, Karen S. "High-Density Nanoenergetic Gas Generators." In Handbook of Nanoscience, Engineering, and Technology, Third Edition, pp. 739-758. CRC Press, 2012.

Johnson, Curtis E., Stephen Fallis, Andrew P. Chafin, Thomas J. Groshens, Kelvin T. Higa,

Ismail MK Ismail, and Tom W. Hawkins. "Characterization of nanometer-to micron-sized aluminum powders: size distribution from thermogravimetric analysis." Journal of propulsion and power 23, no. 4 (2007): 669.

Miziolek, Andrzej. "Nanoenergetics: an emerging technology area of national importance." Amptiac Quarterly 6, no. 1 (2002): 43-48.

Hobosyan, Mkhitar A., and Karen S. Martirosyan. "Iodine Pentoxide Nano rods for High Density Energetic Materials." Propellants, Explosives, Pyrotechnics 42, no. 5 (2017): 506-513.

Hobosyan, Mkhitar A., Srbuhi A. Yolchinyan, and Karen S. Martirosyan. "A novel nano-energetic system based on bismuth hydroxide." RSC Advances 6, no. 71 (2016): 66564-66570.

Nellums,R. R., B. C. Terry, B. C. Tappan, S. F. Son and L. J. Groven, Effect of Solids Loading on Resonant Mixed Al–Bi2O3 Nanothermite Powders, Propellants, Explos., Pyrotech., 2013, 38(5), 605–610.

Oprea, Isabella-Ioana, Hartmut Hesse, and Klaus Betzler. "Optical properties of bismuth borate glasses." Optical Materials 26, no. 3 (2004): 235-237.

Patel, V, K, J. Raj Saurav, K. Gangopadhyay, S. Gangopadhyay and S. Bhattacharya, Combustion characterization and modeling of novel nanoenergetic composites of Co3O4/nAl, RSC Adv., 2015, 5(28), 21471–21479.

Patel, Vinay Kumar, Jayant Raj Saurav, Keshab Gangopadhyay, Shubhra Gangopadhyay, and Shantanu Bhattacharya. "Combustion characterization and modeling of novel nanoenergetic composites of Co_3O_4/nAl." RSC Advances 5, no. 28 (2015): 21471-21479.

Pantoya, Michelle L., and J. J. Granier. "The effect of slow heating rates on the reaction mechanisms of nano and micron composite thermite reactions." Journal of thermal analysis and calorimetry 85, no. 1 (2006): 37-43.

Park, Sunghoon, Soohyun Kim, Gun-Joo Sun, and Chongmu Lee. "Synthesis, structure, and ethanol gas sensing properties of In2O3 nanorods decorated with Bi2O3 nanoparticles." ACS applied materials & interfaces 7, no. 15 (2015): 8138-8146.

Patel, Vinay Kumar, Anurup Ganguli, Rishi Kant, and Shantanu Bhattacharya. "Micropatterning of nanoenergetic films of Bi_2O_3/Al for pyrotechnics." RSC Advances 5, no. 20 (2015): 14967-14973.

Perry, W. Lee, Bettina L. Smith, Christopher J. Bulian, James R. Busse, Clay S. Macomber, Rob C. Dye, and Steven F. Son. "Nano-Scale Tungsten Oxides for Metastable Intermolecular Composites." Propellants, Explosives, Pyrotechnics 29, no. 2 (2004): 99-105.

Puchades, Ivan, Lynn F. Fuller, Sergey E. Lyshevski, Mkhitar Hobosyan, Liu Ting, and Karen S. Martirosyan. "MEMS and 3D-printing microthrusters technology integrated with hydroxide-based nanoenergetic propellants." In Electronics and Nanotechnology (ELNANO), 2017 IEEE 37th International Conference on, pp. 67-70. IEEE, 2017.

Puszynski, Jan A., Christopher J. Bulian, and Jacek J. Swiatkiewicz. "Processing and ignition characteristics of aluminum-bismuth trioxide nanothermite system." Journal of Propulsion and Power 23, no. 4 (2007): 698-706.

Sullivan, Kyle, and Michael Zachariah. "Simultaneous pressure and optical measurements of nanoaluminum thermites: investigating the reaction mechanism." *Journal of Propulsion and Power* 26, no. 3 (2010): 467-472.

Puchades, Ivan, Mkhitar Hobosyan, Lynn F. Fuller, Frank Liu, Siddharth Thakur, Karen S. Martirosyan, and Sergey E. Lyshevski. "MEMS microthrusters with nanoenergetic solid propellants." In Nanotechnology (IEEE-NANO), 2014 IEEE 14th International Conference on, pp. 83-86. IEEE, 2014.

Puszynski, Jan A. "Processing and characterization of aluminum-based nanothermites." Journal of Thermal Analysis and Calorimetry 96, no. 3 (2009): 677-685.

Rogachev, A. S., and A. S. Mukasyan. "Combustion of heterogeneous nanostructural systems." Combustion, Explosion, and Shock Waves 46, no. 3 (2010): 243-266.

Rossi, Carole, Kaili Zhang, Daniel Esteve, Pierre Alphonse, Philippe Tailhades, and Constantin Vahlas. "Nanoenergetic materials for MEMS: a review." IEEE/ASME Journal of Microelectromechanical Systems 16, no. 4 (2007): 919-931.

Rowe, Raymond C., Paul J. Sheskey, and Marian E. Quinn. Handbook of pharmaceutical excipients. Pharmaceutical press, 2009, 11-12

Shiryaev, A. A. (1995). “Thermodynamics of SHS Processes: Advanced Approach,” Int. J. Self-Propag. High-Temp. Synth., 4, 4, 351–362.

Singh, Manish K., Yi Yang, and Christos G. Takoudis. "Synthesis of multifunctional multiferroic

materials from metalorganics." Coordination Chemistry Reviews 253, no. 23 (2009): 2920-2934.

Stamatis, Demitrios, Zhi Jiang, Vern K. Hoffmann, Mirko Schoenitz, and Edward L. Dreizin. "Fully dense, aluminum-rich Al-CuO nanocomposite powders for energetic formulations." *Combustion Science and Technology*181, no. 1 (2008): 97-116.

Tseng, Teng-Kuan, Jihun Choi, Doh-Won Jung, Mark Davidson, and Paul H. Holloway. "Three-dimensional self-assembled hierarchical architectures of gamma-phase flowerlike bismuth oxide." ACS applied materials & interfaces 2, no. 4 (2010): 943-946.

Umbrajkar, Swati M., Mirko Schoenitz, and Edward L. Dreizin. "Control of Structural Refinement and Composition in Al-MoO3 Nanocomposites Prepared by Arrested Reactive Milling." Propellants, Explosives, Pyrotechnics 31, no. 5 (2006): 382-389.

Wang, L., Luss D., and Martirosyan K. S., "The behavior of nanothermite reaction based on Bi_2O_3/Al." Journal of Applied Physics 110, no. 7 (2011): 074311

Wang, Haiyang, Guoqiang Jian, Garth C. Egan, and Michael R. Zachariah. "Assembly and reactive properties of Al/CuO based nanothermite microparticles." *Combustion and Flame* 161, no. 8 (2014): 2203-2208.

Wang, Yi, Wei Jiang, Zhipeng Cheng, Weifan Chen, Chongwei An, Xiaolan Song, and Fengsheng Li. "Thermite reactions of Al/Cu core-shell nanocomposites with WO 3." Thermochimica Acta 463, no. 1 (2007): 69-76.

Wang, L., D. Luss, and K. S. Martirosyan. "The behavior of nanothermite reaction based on Bi2O3/Al." Journal of Applied Physics 110, no. 7 (2011): 074311.

Webster, John G., Halit Eren, R. A. Secco, M. Kostic, and J. R. deBruyn. "Fluid Viscosity Measurement." In Measurement, Instrumentation, and Sensors Handbook, Second Edition: Spatial, Mechanical, Thermal, and Radiation Measurement, pp. 46-1. CRC Press, 2014.

Varma, Arvind, Alexander S. Rogachev, Alexander S. Mukasyan, and Stephen Hwang. "Combustion synthesis of advanced materials: principles and applications." advances in chemical engineering 24 (1998): 79-226.

Xiao, Xin, Shunheng Tu, Chunxia Zheng, Huan Zhong, Xiaoxi Zuo, and Junmin Nan. "l-

Asparagine-assisted synthesis of flower-like β-Bi_2O_3 and its photocatalytic performance for the degradation of 4-phenylphenol under visible-light irradiation." RSC Advances 5, no. 91 (2015): 74977-74985.

Yuan, Dingsheng, Jianghua Zeng, Noel Kristian, Yi Wang, and Xin Wang. "Bi2O3 deposited on highly ordered mesoporous carbon for supercapacitors." Electrochemistry Communications 11, no. 2 (2009): 313-317.

Zhou, Xiang, Daguo Xu, Guangcheng Yang, Qiaobao Zhang, Jinpeng Shen, Jian Lu, and Kaili Zhang. "Highly exothermic and superhydrophobic Mg/fluorocarbon core/shell nanoenergetic arrays." *ACS applied materials & interfaces* 6, no. 13 (2014): 10497-10505.

Zhou, X, M. Torabi, J. Lu, R. Shen and K. Zhang, Nanostructured energetic composites: synthesis, ignition/ combustion modeling, and applications, ACS Appl. Mater. Interfaces, 2014, 6(5), 3058–3074.

Zhou, Lin, Wenzhong Wang, Haolan Xu, Songmei Sun, and Meng Shang. "Bi2O3 hierarchical nanostructures: controllable synthesis, growth mechanism, and their application in photocatalysis." Chemistry–A European Journal 15, no. 7 (2009): 1776-1782.

BIOGRAPHICAL SKETCH

Srbuhi Yolchinyan started an MS in Physics at University of Texas Rio-Grande Valley (UTRGV) in the Fall of 2015 and received her Master's in Physics in Fall 2017. Srbuhi's advisor was Dr. Karen S. Martirosyan. Srbuhi worked in the Advanced Nanoscience Laboratory, her research was focused on novel nano-energetic materials based on metal hydroxides. Srbuhi has no plans to pursue a PhD the following year.

Srbuhi has pursued her Bachelor's degree in Chemistry from Armenian State Pedagogical University after Kh. Abovyan, Yerevan, Armenia, in 2013. Srbuhi has moved to US in 2013 and lived in Brownsville, TX, 401 Ringgold Rd, apt 603, email: srbuhi.yolchinyan01@utrgv.edu. She applied to Graduate Program in Masters of Physics at UTRGV in June 2015 and started her study in Fall. She has successfully conducted research related to nano-energetic materials and presented her research in various conferences. She won best presentation award at Texas Section of American Physical Society's Fall 2015 Presentation Award competition, which was Joint Fall 2015 Meeting of the Texas Sections of the APS/AAPT/Zone 13 of the SPS, Baylor University, Waco, TX. She has also won 1st place in poster competition in Division of Physics during 2017 College of Sciences Annual Conference at UTRGV (March 31, 2017).